AN INVESTIGATION OF THREE DIMENSIONALITY IN HOLOGRAPHIC INTERFEROMETRY

JOHN GERALD SULLIVAN

AN INVESTIGATION OF THREE DIMENSIONALITY IN HOLOGRAPHIC INTERFEROMETRY

by

John Gerald Sullivan
Ensign, United States Navy
B.S., Naval Academy, 1967

Submitted in partial fulfillment of the
requirements for the degree of

MASTER OF SCIENCE IN AERONAUTICAL ENGINEERING

from the

NAVAL POSTGRADUATE SCHOOL

March 1968

ABSTRACT

A discussion of the technique of holography and the laser light sources used therein is presented in this thesis as well as a mathematical description of intensity variation on a hologram due to diffraction and interference effects. Experimental verification is made that a dark-field, two beam hologram acts as a diffraction grating. Finally, the results of an experimental determination of intensity transmission functions for a light-field (diffuse glass) hologram are presented.

TABLE OF CONTENTS

TABLE OF CONTENTS (continued)

LIST OF TABLES

LIST OF ILLUSTRATIONS

LIST OF ILLUSTRATIONS (continued)

ACKNOWLEDGEMENTS

The author wishes to express his deep gratitude to his thesis advisor, Professor Allen E. Fuhs, who, despite a heavy administrative and academic workload, spent a great deal of his time, including several weekends, helping smooth out the rocky areas encountered in the preparation of this thesis. His continuing help and optimism were responsible in no small way for its completion.

Thanks are also due to L. O. Heflinger of TRW Systems. Dr. Heflinger's work in holography is well-known and often referenced. A tour through the facilities of TRW Systems in Redondo Beach, California, helped considerably in developing an understanding of the subject.

Similarly, thanks are due to the staff at Spectra-Physics Corp. of Mountain View, California, for a tour through their facilities and for some valuable information concerning lasers.

Finally, Mr. N. Leckenby and the other technicians of the Department of Aeronautics are to be commended for their interest in, and aid with, the project.

I. INTRODUCTION

Portions of the theory underlying the technique of holographic interferometry are not at present fully understood in their application to the study of variable-density gas dynamics. One of the remaining unsolved problems is to correlate the three-dimensional density distribution about a test object with the amplitude and phase of the resulting intensity pattern on a holographic plate.

In work conducted in the Department of Aeronautics of the Naval Postgraduate School, three approaches to the problem were undertaken:

(1) A comparison of the properties of a dark-field hologram with those of a lined diffraction grating.

(2) An experimental examination of the intensity patterns from a coherently illuminated light-field (diffuse glass) hologram and from the diffuse glass plate used in making the hologram.

(3) Theoretical calculations of the loci of intensity maxima and the intensity contrast due to diffraction near the edges of a square aperture through which has passed coherent laser light. These calculations lead to a dark-field hologram of a square aperture.

An introduction to the holographic process and the laser light sources used therein is included as background material for the studies conducted in this paper.

II. THE HOLOGRAPHIC PROCESS

Dark-Field Holography

Wavefront reconstruction, or holography, is a photographic process by which the amplitude and phase of a complex wave pattern may be recorded and subsequently reproduced. The holographic phenomenon is a consequence of the wave nature of light, first formulated by Christian Huygens (1629-1695). Holographic imagery as such is a product of relatively recent times, developed in its present form initially by Gabor[1] in 1948. A great deal of experimental work has been done with the subject since that time, and a sizable amount of theoretical abstraction has resulted. Among the leaders in the field have been Leith and Upatinieks of the University of Michigan,[2,3] George Stroke,[4] also of the University of Michigan, and the TRW Systems group consisting of Heflinger, Wuerker and Brooks.[5-7]

A great advantage of the holographic method is that it allows an intricate three-dimensional wave pattern to be recorded on a two-dimensional photographic plate, a feature impossible with conventional photography. The hologram, once recorded, may be reconstructed at a more convenient time and examined in great detail. The applications to the field of Aeronautics lie principally at the present time in the area of supersonic and hypersonic flow-field visualization and are just beginning to be realized.[4]

Figure 1 depicts one basic holographic recording and reconstruction process. In Figure 1a, monochromatic, coherent light from a laser

source is fed both directly to a photographic plate (test beam) and to a prism which deflects part of the beam (reference beam) to the plate at an angle to the direct beam. An interference pattern is formed on the photographic plate which becomes essentially a transmission diffraction grating.

After the plate has been developed and returned to the apparatus, it is again illuminated with coherent laser light which is directed parallel to the original test beam. The plate should now exhibit all the properties of a conventional diffraction grating. The spacing between the lines of the grating (or "period" of the grating) is given by the equation:

$$d = \frac{\lambda}{\sin \alpha}$$

where:

d = grating period

λ = wavelength of light used (6328 Å for ~~helium~~ helium-neon laser light)

α = angle between reference and test beams

It can be seen that, for a monochromatic (constant λ) light source, a very finely spaced grating may be made by using a large angle of reference beam incidence. A limit on the fineness of the grating is imposed, however, by the resolution capability of the photographic emulsion. For the experiments discussed in this paper, Kodak 649F glass spectroscopic plates were used which are capable of resolving a maximum of approximately 25,000 lines per inch. An excellent discussion of the efficiency and response properties of

photographic emulsions used in holography is contained in Reference 8.

If an object were placed between the lines A and B in Figure 1a, it would diffract the test beam. The resulting pattern would interfere with the reference beam (which has not impinged upon the object) to form a diffraction pattern at the photographic plate in which are stored the amplitude and phase of the two beams.

To reconstruct the image, the developed photographic plate is illuminated only by the test beam, from which the object has been removed, as shown in Figure 1b. This beam is diffracted by the hologram, and the exact wavefronts of the hologram are reproduced. Real and virtual images of the reconstructed object will appear as shown in Figure 1b. The real image may be projected on a screen but will be of inferior quality unless focusing lenses are employed. An attempt to view the virtual image of the reconstructed object with the naked eye will generally produce unsatisfactory results unless the object is of a highly scattering nature. This is because the pupil of the eye tends to concentrate on the laser beam rather than on the object which will appear relatively dark (hence the term "dark-field holography").

Light-Field Holography

A much more satisfactory way of constructing a hologram for direct viewing is to place a ground glass (diffuse glass) plate in the test beam at position C of Figure 1a during the recording process. The diffuse glass plate and the test object now become the total object. Because

of the ground glass, the object wave at the hologram will be a very complicated function of position. In reconstructing the hologram, the diffuse glass plate will be reproduced; however, since it contains no detail of interest, it serves only to make the test object visible through all parts of the hologram. Holography accomplished in this manner is termed "light-field holography." Figure 2 is a photograph of a light-field hologram containing as test object two pencils crossed at right angles. The image of the pencils is completely encoded in the lines and swirls of the hologram and will not be released until the wave geometry is reconstructed by illumination of the hologram with coherent light.

Double-Exposure Holographic Interferometry

A double-exposure holographic interferogram is made by placing an object in the test section and exposing it with coherent light. A second exposure is then made after a change has been made in the object (for example, a small light-bulb which is turned on between exposures). Interference fringes will result due to the changing aspects of the experiment while the unchanging features will be canceled. Reference 9 contains some excellent photographs illustrating the principle. Using the double-exposure technique, three-dimensional holograms may be recorded in an experimental environment and later reconstructed in more convenient surroundings.

Real-Time Studies

If the two-dimensional aspects of a test scene are of interest, the relatively simple technique of "real-time" holographic interferometry may be used. A dark-field hologram is made as shown in Figure 1a with no test object present. After development, a test scene is introduced between the hologram and the reconstructing laser light source. Photographs may then be taken in real time of the resulting interference fringes using a high speed film such as Poloroid "3000." References 10 and 11 describe applications of the real-time technique to supersonic wind-tunnel studies.

Further Applications of Holography

Acoustical holography,[12-14] in which acoustically generated electrical impulses are transferred to the visual frame of reference (for example, by means of an oscilloscope) and recorded in three dimensions using holographic interferometry, is being intensively investigated. The military applications in the domain of anti-submarine warfare (ASW)[12] seem very promising at this time. It is easy to imagine an extension of the technique from sonar (sound) generated holograms to those generated by radar, providing, for example, a continuous three-dimensional picture of the terrain ahead for the pilot of a low-flying combat jet.

Research is also being conducted into both military and commercial applications of holography to the field of communications.[3,14] Stroke,[15] of the University of Michigan, reports success in constructing full color

holograms on black-and-white film by illuminating an object with laser light of different colors. Reconstruction of the object occurs when ordinary white light illuminates the hologram. He foresees the possibility of a future television set which will hang on a wall like a picture through which three-dimensional programs may be viewed, with the picture appearing much as the scene would in real life when observed through a clear glass window.

III. LASERS

Prior to the development of the laser (Light Amplification by Stimulated Emission of Radiation), the entire holographic process was primarily of academic interest due to the lack of adequate light sources and the unavailability of photographic emulsions with the requisite high resolution characteristics. Following the development of the first practical laser in 1960,[16] however, emulsions suitable for holographic purposes began to appear in a relatively short time. The first commercially available (and still most widely used) were the Kodak 649F glass spectroscopic slides, the resolution capability of which was discussed in the previous section.

The properties of the laser which makes it suitable for holography are its high degree of temporal and spatial coherence and, for many applications, its ability to produce a beam in the visible spectrum.[17] The spatial coherence and time coherence of the laser allow an interference pattern to be formed by suitable routing of the laser beam through optical arrangements utilizing prisms or mirrors.

The Gas Laser

Probably the most widely used laser at the present time is the gas laser.[16] The first research in the field was concerned with gas lasers primarily because relations between the energy levels of many gases were better understood than those with solid-state materials. Curiously, the ruby laser was discovered first,[5] but the development of the gas laser soon followed.

Javan, Bennett, and Herriott[16] developed the helium-neon laser in 1960, and since that time extensive research has been conducted utilizing other gas sources. Practical holography essentially began with the discovery of the 6328 angstrom line from helium-neon. The laser producing this line differed only slightly from the first gas laser,[16] and its great advantage for laboratory investigations lay in the fact that the light produced was in the visible portion of the spectrum. Much subsequent effort was devoted to increasing the power output of the beam both with the helium-neon source and with other gas sources. The highest continuous power gas laser available at the present time is the CO_2 laser, the maximum output of which can be of the order of several hundred watts. Pulsed gas lasers, as opposed to continuous wave (CW) output, have been developed which produce considerably higher power but have intermittent operation. Table I lists most of the gas lasers available at the present time and presents some of the characteristics of each.

The Solid-State Laser

In general, a solid state laser material will consist of a transparent binder material such as glass or quartz into which is fused a relatively small amount of an active florescent ion such as Cr^3 or Nd^3.[18] By far the greatest amount of research has been done with ruby laser material which uses the physical characteristics of the chromium ion to produce and amplify a coherent light signal. This ion, whose lifetime is long by atomic standards, can be "pumped up" to higher energy levels by

means of an intense white light source. These energy levels are limited by quantum theory to certain discrete levels, the lowest of which is termed the "ground state."

The Cr^3 ion will remain in the excited state only briefly and in returning to lower levels will emit a photon whose wavelength is determined by the energy change of the transition. The decay to lower energy levels can occur spontaneously; but, in practice, almost all decay occurs when a photon previously emitted moves through the ruby material and stimulates emission of another photon. In essence, then, a "chain reaction" takes place resulting in output amplification. Practically all light radiation in properly manufactured ruby laser material occurs between a dominantly excited energy level at 6943 A and the ground state of the Cr^3 ion. It is this fact, together with the fact that each new photon emission occurs in phase with previously emitted photons, which accounts for the highly monochromatic, coherent light output. In addition, the light rays of the laser output beam are made very nearly parallel by forming the laser material into a circular rod cross-section with a large length-to-diameter ratio. Any photons with a significant radial velocity component, therefore, will leave the rod before traveling very far in the beam direction.

With both the gas and solid-state lasers, much higher power output is obtainable in the pulsed mode of operation than in the continuous wave mode. This is a distinct advantage in holographic applications where motion is involved (such as ballistic range studies)

because the photographic emulsions with the necessary high resolution characteristics for holography have, in general, very low sensitivity; i.e., the ASA number of Kodak 649F plates is 1/300. A very brief, intense pulse is required, therefore, if the motion is to be stopped and the plate adequately exposed.

IV. EXPERIMENTAL APPARATUS

The holographic interferometer in use at the Naval Postgraduate School was built in conjunction with previous experiments with holography.[10,11] It utilizes a Spectra-Physics Model 124 continuous wave helium-neon laser as a coherent light source. The Model 124 laser has a rated power output of 15 milliwatts at a wavelength of 6328 angstroms in the visible red portion of the spectrum. The output beam has a divergence of 0.057 degrees. A Spectra-Physics Model 331 collimating lens and spatial filter, which attaches to the output end of the laser, was used in order to expand the 1.1 millimeter diameter output beam of the basic laser to approximately 3.5 inches. Further beam expansion was accomplished by using a double-concave lens with a negative 10 centimeter focal length and an 8 inch double-convex collimating lens. The resulting beam at the holographic plate was approximately 6 inches in diameter, more than adequate to cover the 4 X 5 inch Kodak 649F spectroscopic plates used in the experiments.

A plexiglass prism was placed in the expanded output beam between the test section and the hologram in order to provide the reference beam. The prism dimensions were 4 X 6 inches, and the prism refracted one-half of the laser output beam by an angle of 10.5 degrees, thus providing for superposition of the test and reference beams at the holographic plate.

An L-shaped aluminum plate holder was constructed so that the holograms could be exposed and returned precisely to their original position after developing.

All components were mounted on a 10 foot long standard optical bench supported for structural rigidity by a 4 X 8 inch aluminum I beam. The entire apparatus rested at different times on a laboratory table or on several desks. Figure 3 is a photograph of the setup used for making holograms.

Intensity measurements were made using an Eldorado Model 30 Differential Photometer. Figure 4 is a photograph of the layout used for making the measurements.

V. DISCUSSION OF EXPERIMENTAL PROCEDURE AND RESULTS

The Hologram as a Diffraction Grating

At the outset of the investigations, the question was present as to whether the simple, dark-field hologram does in fact behave as a diffraction grating. In order to answer the question, a dark-field hologram (with no test object present) was exposed as shown in Figure 1a.

Reconstruction was accomplished utilizing the direct beam of the laser which provided essentially a point source of illumination. The hologram was rotated about the horizontal axis (the axis parallel to the lines of the grating) as illustrated in Figure 5. The angles of diffraction, θ_I, for the n = 0 and n = 1 orders were plotted as a function of the hologram rotation angle, θ_H. The results, shown in Figures 5 and 6, within experimental error, are those predicted by diffraction grating theory (See Appendix). This demonstrates that the ability of the simple, dark-field hologram to diffract the incident beam into the various orders is similar to that of the mechanically lined diffraction grating.

Intensity Variation of the Dark-Field Hologram

Givens[19] puts forth the hypothesis that if the transmitted amplitude of the simple, dark-field hologram behaves as a sine wave according to the expression

$$A_T = a + b \cos qy \qquad (1)$$

then the intensity in the various orders has certain values. In Equation (1) the symbols are assigned the following meaning:

A_T = transmitted amplitude

y = the coordinate normal to the lines of the grating and in the plane of the grating

q = $2\pi d$ where d is the grating spacing

a = a constant determining the average transmission of the grating

b = a constant determining the contract of the grating

According to Givens, the hologram, behaving as a diffraction grating according to Equation (1), will diffract into the zero order light of amplitude a and into the first order on each side light of amplitude b/2. Also there should be zero intensity in orders with $n > 1$.

A check was made with several dark-field holograms to see whether they behaved according to Givens' hypothesis. The amplitude of the orders to each side of the zero order were not found to be equal; rather, their relative value differed by 10 to 20 per cent, depending upon the hologram tested. It is felt that perhaps an uneven application of the photographic emulsion to the holographic plate is sufficient to account for the discrepancies noted. Nonlinear response of the emulsion to light could cause deviation from a cosine distribution.

Intensity Variation of the Light-Field Hologram and of Diffuse Glass

One of the unsolved problems in holographic interferometry at the present time is the determination of the relationship between the light intensity of a reconstructed wave from a hologram and the three-

dimensional gas density surrounding a test object such as a match or a wind-tunnel model. Knowledge of this relationship will enable one to measure density at a given point.

To understand the rationale leading to the experiments, consider the following physical description of the reconstruction of a light-field hologram as illustrated in Figure 7. A coherent laser beam of intensity $I_O(x,y)$ impinges on a diffuse glass plate and is modified by the transmission function, T_D, of the diffuse glass, defined as:

$$T_D(x,y,\alpha) = \frac{\text{intensity at angle } \alpha}{\text{intensity at } x,y}$$

The beam leaving the diffuse glass, $I_D(x',y')$, passes through a light-field hologram, the transmission function of which is defined as:

$$T_H(x',y',\beta) = \frac{\text{intensity at angle } \beta}{\text{intensity at } x',y'}$$

The resulting intensity at point P of the beam, $I_H(x'',y'')$, after having passed through both the diffuse glass plate and the light-field hologram is:

$$I_H(x'',y'') = I_O(x,y)T_D(x,y,\alpha)T_H(x',y',\beta)$$

The superposition of all beams, $I_O(x,y)$, impinging on the diffuse glass plate and passing through the point, x',y', of the light-field hologram forms an intensity pattern as illustrated in Figure 8. The final reconstruction of the light-field hologram depends upon an analysis of the intensity pattern from light passing through all parts of the

hologram at all angles, γ . As a first step in this direction, two experiments were undertaken.

First, a light-field (diffuse glass) hologram was constructed as shown in Figure 9a. After being developed, it was returned to the plate holder and the wave reconstructed (1) with the hologram at normal incidence ($\theta_H = 0$) to the test beam as shown in Figure 9b and (2) with the hologram rotated about a horizontal axis in order to produce angles of incidence, θ_H, to the test beam as illustrated in Figure 10a. Clockwise and counterclockwise hologram rotation angles, θ_H, of 10 and 20 degrees were used. Relative intensity measurements were then taken as a function of the polar angle, α , utilizing the Differential Photometer described in Section IV. The results are shown in Figures 11 through 13.

Second, the diffuse glass plate used in making the light field hologram described above was illuminated with coherent laser light as shown in Figure 10b. Again using the Eldorado Photometer measurements were taken of relative intensity as a function of the polar angle, α . The results are plotted in Figure 14. It was expected that a Gaussian distribution for the transmission function,

$$T_D(\alpha) = Ce^{-\beta^2 x^2}, \quad (\beta = \text{a constant})$$

would be obtained where, in the coordinates of the experiment, $x = \tan\alpha$ and C is a constant. This was not the case, however; instead, the transmission distribution most closely approximated curves represented

by the equation

$$T_D(\alpha) = Ce^{-\beta \tan \alpha}$$

where, again, $x = \tan \alpha$. Figure 15 shows that values of β near 8.0 were closest to the experimental intensity distribution.

If the diffuse glass plate and the light-field hologram were combined, the resulting intensity distribution should appear as sketched in Figure 8. An analysis of this kind, although not carried out by the author due to time restrictions, should prove extremely interesting in the future as a step toward explaining the three-dimensional aspects of light-field holographic interferometry.

VI. FRESNEL DIFFRACTION BEYOND A RECTANGULAR APERTURE

The theoretical calculations of this section are carried out as a first step toward the solution of the more difficult problems previously mentioned involving variable-density flow fields.

The Kirchhoff Differential,[20] which describes the diffraction beyond the rectangular aperture of Figure 16, is given by:

$$d\tilde{E}_P = \frac{j\mathcal{E}_o}{\lambda r} e^{j\omega(t-\frac{r}{c})} \left\{ \frac{1+\cos\theta}{2} \right\}$$

where:

$d\tilde{E}_p$ = complex amplitude

$\mathcal{E}_o$ = amplitude at aperture

λ = wavelength

r = distance from dS to P

c = speed of light

ω = angular frequency in radians/sec.

θ = angle measured from normal to dS to the r vector extending from dS to P

$\sim$ implies a complex expression

From the geometry of Figure 16,

$$r^2 = r_o^2 + (x - x_p)^2 + (y - y_p)^2$$

or:

$$r^2 = r_o \left\{ 1 + \left(\frac{x - x_p}{r_o} \right)^2 + \left(\frac{y - y_p}{r_o} \right)^2 \right\}$$

For the special case where:

$$\left(\frac{x - x_p}{r_o} \right)^2 << 1 \quad ; \quad \left(\frac{y - y_p}{r_o} \right)^2 << 1$$

then:

(a) $r \cong r_0$

(b) θ is small.

Therefore, the obliquity factor,[20]

$$\left\{ \frac{1 + \cos\theta}{2} \right\}$$

from Equation (2) is approximately equal to 1 and may be ignored.

With the above assumptions, Equation (2), when integrated over the aperture, becomes:

$$\tilde{E}_p = \frac{j\mathcal{E}_0}{\lambda r_0} \int_{-x_0}^{x_0} \int_{-y_0}^{y_0} e^{-j\omega\left(t - \frac{r_0}{c}\right)} e^{-j\frac{\omega}{c}\left[\frac{(x - x_p)^2}{2r_0}\right]} e^{-j\frac{\omega}{c}\left[\frac{(y - y_p)^2}{2r_0}\right]} dx\,dy \qquad (4)$$

Since the angular frequency, ω, is related to the wavelength of the incident light, λ, by

$$\omega = 2\pi \frac{c}{\lambda}$$

and since the first exponential is independent of x and y, Equation (4) becomes:

$$\tilde{E}_p = \frac{j\mathcal{E}_0 e^{-j\omega\left(t - \frac{r_0}{c}\right)}}{\lambda r_0} \int_{-x_0}^{x_0} e^{-j2\pi\left[\frac{(x - x_p)^2}{2\lambda r_0}\right]} dx \int_{-y_0}^{y_0} e^{-j2\pi\left[\frac{(y - y_p)^2}{2\lambda r_0}\right]} dy$$

or:

$$\tilde{E}_p = \frac{j\mathcal{E}_0 e^{\left(t - \frac{r_0}{c}\right)}}{2} \sqrt{\frac{2}{\lambda r_0}} \int_{-x_0}^{x_0} e^{-j2\pi\left[\frac{(x - x_p)^2}{2\lambda r_0}\right]} dx \sqrt{\frac{2}{\lambda r_0}} \int_{-y_0}^{y_0} e^{-j2\pi\left[\frac{(y - y_p)^2}{2\lambda r_0}\right]} dy \qquad (5)$$

Defining quantities u^2 and w^2:

$$u^2 \equiv \frac{(x-x_p)^2}{\lambda r_0/2} \quad , \quad u = \frac{(x-x_p)}{\sqrt{\lambda r_0/2}} \quad , \quad du = \frac{dx}{\sqrt{\lambda r_0/2}}$$

$$w^2 \equiv \frac{(y-y_p)^2}{\lambda r_0/2} \quad , \quad w = \frac{(y-y_p)}{\sqrt{\lambda r_0/2}} \quad , \quad dw = \frac{dy}{\sqrt{\lambda r_0/2}}$$

Equation (5) becomes:

$$\tilde{E}_p = \frac{j\varepsilon_0}{2} e^{-j\omega(t-\frac{r_0}{c})} \int_{-x_0}^{x_0} e^{-j\frac{\pi}{2}u^2} du \int_{-y_0}^{y_0} e^{-j\frac{\pi}{2}w^2} dw \qquad (6)$$

To express the limits of integration in Equation (6), define the following quantities:

(a) $$u_2(x_0, x_p) \equiv \frac{x_0 - x_p}{\sqrt{\lambda r_0/2}}$$

(b) $$u_1(x_0, x_p) \equiv -\frac{x_0 + x_p}{\sqrt{\lambda r_0/2}} \qquad (7)$$

(c) $$w_2(y_0, y_p) \equiv \frac{y_0 - y_p}{\sqrt{\lambda r_0/2}}$$

(d) $$w_1(y_0, y_p) \equiv -\frac{y_0 + y_p}{\sqrt{\lambda r_0/2}}$$

The first integral of Equation (6) may be split into two parts:

$$\tilde{X} \equiv \int_{-x_0}^{x_0} e^{-j\frac{\pi}{2}u^2} du = \int_0^{x_0} e^{-j\frac{\pi}{2}u^2} du - \int_0^{-x_0} e^{-j\frac{\pi}{2}u^2} du$$

$$= \int_0^{u_2} e^{-j\frac{\pi}{2}u^2} du - \int_0^{u_1} e^{-j\frac{\pi}{2}u^2} du \qquad (8)$$

Defining the Fresnel Integrals $\mathcal{C}(u)$ and $\mathcal{S}(u)$:

$$\mathcal{C}(u) \equiv \int_0^u \cos \tfrac{\pi}{2} u^2$$

$$\mathcal{S}(u) \equiv \int_0^u \sin \tfrac{\pi}{2} u^2$$

Equation (8) becomes:

$$\begin{aligned} \tilde{X} &= \mathcal{C}(u_2) - j\,\mathcal{S}(u_2) - \mathcal{C}(u_1) + j\,\mathcal{S}(u_1) \\ &= \left[\mathcal{C}(u_2) - \mathcal{C}(u_1)\right] - j\left[\mathcal{S}(u_2) - \mathcal{S}(u_1)\right] \\ &= \Delta\mathcal{C}_x - j\,\Delta\mathcal{S}_x \end{aligned}$$

or:

$$\tilde{X} = \sqrt{\Delta\mathcal{C}_x^2 + \Delta\mathcal{S}_x^2}\; e^{-j \tan^{-1} \frac{\Delta\mathcal{S}_x}{\Delta\mathcal{C}_x}}$$

The derivation of the second integral of Equation (6) in terms of the Fresnel Integrals is entirely analogous. Finally, defining the first term of Equation (6) as:

$$\tilde{Z} \equiv \frac{j\varepsilon_0}{2}\, e^{-j\omega\left(t - \frac{r_0}{c}\right)}$$

Equation (6) becomes the complex product

$$\tilde{E}_p = \tilde{Z}\,\tilde{X}\,\tilde{Y} \qquad (9)$$

where:

$$\tilde{X} = \sqrt{\Delta C_x^2 + \Delta S_x^2}\; e^{-j \tan^{-1} \frac{\Delta S_x}{\Delta C_x}}$$

$$\tilde{Y} = \sqrt{\Delta C_y^2 + \Delta S_y^2}\; e^{-j \tan^{-1} \frac{\Delta S_y}{\Delta C_y}}$$

Cornu's Spiral,[20] shown in Figure 17, is a beautiful method for describing the $\mathbb{C}$ and $\mathbb{S}$ integrals by means of their complex conjugates. Table II contains values of the integrals for certain numerical values of u. It can be seen from Figure 17 that the plus and minus "eyes" of the spiral occur for $u \rightarrow +\infty$ and $u \rightarrow -\infty$ respectively in which case the following relations hold:

$$\lim_{u \rightarrow \pm\infty} \int \cos \tfrac{\pi}{2} u^2 \, du = \pm 0.5$$

$$\lim_{u \rightarrow \pm\infty} \int \sin \tfrac{\pi}{2} u^2 \, du = \pm 0.5$$

VII. CALCULATION OF A HOLOGRAM FOR A SQUARE APERTURE

Solution for Region "A"

Consider Region "A" of Figure 18. Coherent, parallel light from a laser source passes through both the prism and the aperture in Plane 1 and impinges on Plane 2. Consider the beam, a_o, through the aperture:

$$a_o = \tilde{Z}\tilde{X}\tilde{Y}$$

$$= \left[\frac{j\mathcal{E}_o}{2} e^{-j\omega(t-\frac{r_o}{c})}\right]\left[\sqrt{\Delta\mathcal{C}_x^2 + \Delta\mathcal{S}_x^2}\, e^{-j\tan^{-1}\frac{\Delta\mathcal{S}_x}{\Delta\mathcal{C}_x}}\right]\left[\sqrt{\Delta\mathcal{C}_y^2 + \Delta\mathcal{S}_y^2}\, e^{-j\tan^{-1}\frac{\Delta\mathcal{S}_y}{\Delta\mathcal{C}_y}}\right] \quad (10)$$

For a sample calculation, let:

r_o = 10 cm.

$x_o = y_o$ = 1 cm.

$\lambda = 2 \times 10^{-5}$ cm.

θ = 20 degrees

$\mathcal{E}_o$ = 1 unit of amplitude

Choose a time, t, such that

$$\omega\left(t - \frac{r_o}{c}\right) = 0$$

From Equation (7):

$$u_2(y_o, y_p) = \frac{y_o - y_p}{\sqrt{\lambda r_o/2}} = \frac{1}{\sqrt{\frac{(2\times10^{-5}\text{CM})(10\text{CM})}{2}}} = +200$$

and

$$u_1(y_o, y_p) = -\frac{y_o + y_p}{\sqrt{\lambda r_o/2}} = -\frac{1}{\sqrt{\frac{(2\times10^{-5}\text{CM})(10\text{CM})}{2}}} = -200$$

which are nearly in the respective "eyes" of the Cornu Spiral of Figure 17.

Therefore:

$$\Delta C_y = 1$$

$$\Delta S_y = 1$$

and Equation (10) becomes, using $j = \exp(j\frac{\pi}{2})$:

$$\tilde{a}_o = \frac{1}{2}\left[\sqrt{\Delta C_x^2 + \Delta S_x^2}\, e^{-j\tan^{-1}\frac{\Delta S_x}{\Delta C_x}}\right]\left[\sqrt{2}\, e^{+j\frac{\pi}{4}}\right]$$

Therefore:

$$\tilde{a}_o = \sqrt{\Delta C_x^2 + \Delta S_x^2}\; e^{j\left(\frac{\pi}{4} - \tan^{-1}\frac{\Delta S_x}{\Delta C_x}\right)} \qquad (11)$$

where:

$$a_o = \sqrt{\Delta C_x^2 + \Delta S_x^2}$$

$$\phi = \left(\frac{\pi}{4} - \tan^{-1}\frac{\Delta S_x}{\Delta C_x}\right)$$

Next, consider the reference beam, $\tilde{a}_r$, which may be represented by:

$$\tilde{a}_r = a_r e^{j\psi} \qquad (12)$$

If the phase of $\tilde{a}_r(x_o, o, r_o)$ is set equal to the phase of $\tilde{a}_o(x_o, o, r_o)$, then the phase of a_r along the hologram (plane 2) in the y direction is given by:

$$\psi = \frac{2\pi y' \sin\theta}{\lambda}$$

where:

$$y' = (y_o - y)$$

Since, in experimental holography, the best results are obtained when the amplitude of the reference beam is somewhat greater than the amplitude of the test beam, set

$$|\tilde{a}_r| = 3|\tilde{a}_o|$$

Therefore, at the aperture of Figure 18:

$$\tilde{a}_r = 3e^{j\left(\frac{2\pi y' \sin\theta}{\lambda}\right)} \tag{13}$$

where:

$$a_r = 3 \quad ; \quad \Psi = \frac{2\pi y' \sin\theta}{\lambda}$$

The amplitude at the hologram, $\tilde{a}$, is the complex sum of $\tilde{a}_r$ and $\tilde{a}_o$. That is:

$$\tilde{a} = \tilde{a}_r + \tilde{a}_o$$

The intensity, I, at the hologram (plane 2) is:

$$\begin{aligned} I &\equiv \tilde{a}\tilde{a}^* \\ &= (a_r \cos\Psi + a_o \cos\phi)^2 + (a_r \sin\Psi + a_o \sin\phi)^2 \\ &= a_r^2 + a_o^2 + 2a_r a_o \cos(\Psi - \phi) \end{aligned} \tag{14}$$

where $\tilde{a}^*$ is the complex conjugate of $\tilde{a}$.

Minimum intensity occurs for:

$$(\psi - \phi) = (2n-1)\pi \qquad \pm n = 0, 1, 2, \cdots$$

and:

$$I_{min} = (a_r - a_0)^2 \tag{15}$$

Similarly, maximum intensity (and hence maximum photographic darkening) occurs for:

$$(\psi - \phi) = 2n\pi \qquad \pm n = 0, 1, 2, \cdots$$

and:

$$I_{MAX} = (a_r + a_0)^2 \tag{16}$$

For I_{max}

$$(\psi - \phi) = 2n\pi$$

Therefore, using Equations (11) and (12):

$$\frac{2\pi y' \sin\theta}{\lambda} - \left(\frac{\pi}{4} - \tan^{-1}\frac{\Delta S_x}{\Delta C_x}\right) = 2n\pi \tag{17}$$

For the case n = 0, Equation (17) becomes:

$$\frac{2\pi y' \sin\theta}{\lambda} - \left(\frac{\pi}{4} - \tan^{-1}\frac{\Delta S_x}{\Delta C_x}\right) = 0$$

or:

$$y'/\lambda = \frac{\frac{\pi}{4} - \tan^{-1}\frac{\Delta S'_x}{\Delta C_x}}{2\pi \sin\theta}$$

Since $\theta = 20$ degrees was chosen for the sample calculation, the above equation becomes:

$$y'/\lambda = \frac{45^\circ - \tan^{-1}\frac{\Delta S'_x}{\Delta C_x}}{123^\circ} \qquad (18)$$

y'/λ is plotted as a function of u_2 in Figure 19. The necessary calculations are summarized in Tables III and IV.

Contrast is defined as:

$$\text{contrast} = \frac{I_{max} - I_{min}}{I_{max} + I_{min}}$$

Since the amplitude of the reference beam was set at three times the amplitude of the test (aperture) beam (i.e., $a_r = 3a_o$), Equations (15) and (16) reduce to:

$$I_{MIN} = a_o^2 - 6a_o + 9$$

$$I_{MAX} = a_o^2 + 6a_o + 9$$

Then:

$$\text{contrast} = \frac{6a_o}{9 + a_o^2}$$

Contrast is plotted as a function of u_2 in Figure 20 with the calculations given in Tables III and IV.

Figure 21 is a graphical sketch combining the results from Figures 19 and 20. Within the aperture (u_2 positive), contrast is high and the lines of maximum intensity oscillate about the line, $y/\lambda = 0$, with decreasing oscillation toward the center of the aperture. Outside the aperture (u_2 negative), the lines of maximum intensity bend sharply in the negative y/λ direction and contrast falls off greatly. At $u_2 = -1.9$, the contrast is only about 15 per cent of that at $u_2 = +1.2$.

Solution for Region "B"

The complex amplitude of the reference beam, from Equation (12) is:

$$\tilde{a}_r = a_r e^{i\Psi}$$

From the geometry of Figure 13, the phase of the reference beam, which is not affected by the aperture, at Plane 2 is given by:

$$\frac{2\pi y \sin\theta}{\lambda} = 2n\pi$$

The equation for the test beam, from Equation (11), is:

$$\tilde{a}_o = a_o e^{i\Phi}$$

where:

$\Phi = 0$ if no aperture is present and

$\Phi = \pi - 4 \frac{\Delta S}{\Delta C}$ with the aperture present.

Consider the case of no aperture. For location of the intensity maxima:

$$\psi - \Phi = 0$$

and the spacing of the resulting maxima is given by:

$$\frac{2\pi y'' \sin\theta}{\lambda} = 2n\pi \tag{19}$$

where y" is measured from the origin.

With the aperture present, the condition for maximum intensity:

$$\psi - \Phi = 0$$

yields

$$\frac{2\pi y \sin\theta}{\lambda} - \left(\frac{\pi}{4} - \tan^{-1}\frac{\Delta\xi'}{\Delta\eta'}\right) = 2n\pi \tag{20}$$

Subtracting Equation (19) from Equation (20) gives the spacing of the intensity maxima along the y axis relative to the position of the lines with no aperture in Region "B":

$$\frac{2\pi \Delta y \sin\theta}{\lambda} - \left(\frac{\pi}{4} - \tan^{-1}\frac{\Delta\xi'}{\Delta\eta'}\right) = 0 \tag{21}$$

where:

$$\Delta y = y - y''$$

It can be seen that Equation (21) is identical to Equation (17) if y' is replaced by Δy. The spacing of the lines of maximum can therefore be read from Figure 19 by replacing u_2 by w_2 and y/λ by $\Delta y/\lambda$.

The solution for contrast in Region "B" is identical to that for Region "A" and can be read from Figure 20 by replacing the abscissa, u_2, by w_2.

Figure 22 is a sketch combining the spacing of the lines of maximum intensity and the contrast in Region "B".

VIII. SUMMARY AND RECOMMENDATIONS

During the course of the investigations, it was discovered that the technique of constructing acceptable holograms, which seems a fairly simple process in theory, requires in practice the mastery of a rather sizable amount of trial-and-error experimentation. Once some degree of mechanical proficiency is acquired, however, repeatably good results can be obtained.

High quality and accurate alignment of the optical components, critical factors in Schlieren and Mach-Zehnder systems performing in somewhat the same capacity as the holographic interferometer, were not necessary. The prism used to provide the reference beam for making the holograms, for example, was of ordinary plexiglass and had been made and polished by hand for use in conjunction with previous work conducted with holography at the Naval Postgraduate School.

Because of the very fine spacing of the lines on a hologram (on the order of 0.001 cm.), all holograms were made at night when vibration due to traffic and operating machinery was at a minimum.

As a result of experiments conducted, the conclusion was reached that the simple, dark-field hologram behaves as a mechanically lined diffraction grating insofar as angular diffraction is concerned but does not give a sinusoidal intensity distribution in accordance with the Givens' hypothesis of Section V.

Data were taken and curves plotted for the angular distribution of relative amplitude for the case of both a light-field (diffuse glass)

hologram and the diffuse glass plate which was used to make the hologram. The diffuse glass plate did not yield a Gaussian intensity distribution as expected, which, in the coordinates of the experiment, would have been represented by

$$\text{intensity} = e^{-(\text{constant})\tan^2 \alpha}$$

where α is a measure of the angular spread from the impinging laser beam, but gave rather a curve most closely approximated by

$$\text{intensity} = e^{-(\text{constant})\tan \alpha}$$

It is regretted that further investigation of the light-field hologram could not be carried out in the time available nor theory developed to explain the rather unusual results of Figures 9 through 11.

A detailed mathematical description of Fresnel diffraction of coherent light at the edges of a square aperture was presented, however, which, with further expansion, may suffice to explain the three-dimensional aspects of the light field (diffuse glass) holographic interferogram.

The author has the following to offer by way of recommendations:

(1) That further experimentation and corresponding theoretical abstraction be undertaken in light-field holography, with the goal of obtaining a more complete understanding of the three-dimensional aspects involved, and

(2) That experiments in multi-color holography be undertaken using the School's newly acquired "green beam" argon laser in conjunction with the Spectra-physics "red beam" helium-neon laser used for the experiments discussed in this thesis.

REFERENCES

1. D. Gabor, "A New Microscopic Principle," Nature, 161 (May, 1948), p. 777.

2. E. N. Leith and J. Upatneiks, "Wavefront Reconstruction with Diffused Illumination and Three-Dimensional Objects," J. Opt. Soc. of Amer., 54 (1964), pp. 1295-1301.

3. E. N. Leith and J. Upatneiks, "Reconstructed Wavefronts and Communication Theory," J. Opt. Soc. of Amer., 52 (October, 1962), pp. 1123-1130.

4. George W. Stroke, An Introduction to Coherent Optics and Holography, Academic Press, New York, 1966.

5. R. E. Brooks, L. O. Heflinger, R. F. Weurker, and R. A. Briones, "Holographic Photography of High-Speed Phenomena with Conventional and Q-Switched Ruby Lasers," Applied Physics Letters, 7 (1965), pp. 248-249.

6. R. E. Brooks, R. F. Weurker, L. O. Heflinger, and C. Knox, "Holographic Interferometry with Applications to Fluid Mechanics," Paper presented at the International Symposium on Gasdynamics of Explosions, Brussels, Belgium, September 20, 1967.

7. L. O. Heflinger, R. F. Weurker, and R. E. Brooks, "Holographic Interferometry," J. App. Phys., 37 (February, 1966), pp. 642-649.

8. H. Kogelnik, "Hologram Efficiency and Response," Laser Technology, 5 (November, 1967), pp. 68-73.

9. Robert E. Brooks, "New Dimension for Interferometry," Electronics, 12 (May 15, 1967), pp. 88-93.

10. J. H. Holds, "Aeronautical Applications of Holographic Interferometry," M. S. Thesis, Department of Aeronautics, Naval Postgraduate School, Monterey, California, June, 1967.

11. J. H. Holds and A. E. Fuhs, "A Refined Analysis of a Holographic Interferogram," J. App. Phys., 38 (December, 1967), pp. 5408-5409.

12. "Making 3-D Pictures with Sound," Time, 90 (Nov. 10, 1967), pp. 66-67.

13. A. F. Metherell, H. M. A. El-Sum, J. J. Dreher, and L. Larmore, "Image Reconstruction from Sampled Acoustical Holograms," Applied Physics Letters, 10 (May 15, 1967), pp. 277-279.

14. J. D. Young and J. E. Wolfe, "A New Recording Technique for Acoustic Holography," Applied Physics Letters, 11 (November 1, 1967), pp. 294-296.

15. "Pure Light for Practical Pictures," Time, 89 (March 18, 1966), p. 60.

16. A. L. Bloom, "Gas Lasers," Applied Optics, 5 (October, 1966), pp. 1501-1511.

17. J. M. Stone, Radiation and Optics, McGraw-Hill, New York, 1963, Chapter 10.

18. Gerald B. Steel, "High Speed Schlieren Photography using a Kerr Cell Modulated Laser Light Source," AIAA Student Journal, 4 (October, 1966), pp. 82-85.

19. M. Parker Givens, "Introduction to Holography," J. App. Phys., 38 (May, 1967), pp. 1056-1064.

20. John Strong, Concepts of Classical Optics, W. H. Freeman and Company, San Francisco, 1958, Chapter IX.

21. Ralph A. Sawyer, Experimental Spectroscopy, Prentice-Hall, New York, 1946, pp. 122, 159-161.

TABLE I. PROPERTIES OF REPRESENTATIVE GAS LASERS

Wavelength microns	Medium	Operation	Design Parameters			Comments
			Length	Power In	Power Out	
0.2358	NeIV	Pulsed	1 meter	15 MW peak	—	Shortest wavelength known in laser transition. Requires large currents.
0.3324	NeII	Pulsed	1 meter	300 watts avg.	10 mW	Other NeII and ArIII lines obtainable on same basis in this wavelength region.
0.3371	N_2	Pulsed	2 meters	10 watts/pulse	200 kW peak	Requires very high voltages.
0.4880	ArII	CW	60 cm	5 kW	1 watt	High power visible - blue.
0.5145	ArII	CW	60 cm	5 kW	1 watt	High power visible - green.
0.5682	KrII	CW	60 cm	3 kW	0.5 watt	Strong line in yellow part of spectrum.
0.6150	HgII-He	Pulsed	60 cm	50 watts avg.	100 mW	Narrow Doppler width - good interferometer source
0.6328	He-Ne	CW	15 cm	10 watts	0.1 mW	Single frequency - wavelength standard.
0.6328	He-Ne	CW	2 meters	100 watts	100 mW	General purpose - high power red.
1.1523	He-Ne	CW	2 meters	100 watts	40 mW	General purpose.
2.0261	Xe	CW	2 meters	100 watts	10 mW	High gain.
3.3912	He-Ne	CW	2 meters	100 watts	20 mW	Very high gain per pass - competition with 0.6328 useful in plasma interferometry.
3.507	Xe	CW	1 meter	50 watts	1 mW	Very high gain.
10.6	CO_2-N_2-He	CW or Q-sw.	2 meters	1000 watts	100 watts	High efficiency and high power.
27.9	H_2O	Pulsed	1 meter	100 watts	10 watts peak	
118.6	H_2O	Pulsed	1 meter	100 watts	1 mW	

Reproduced from "Gas Lasers" by A.L.Bloom, Applied Optics, 5 (Oct., 1966.) P. 1502.

TABLE II

CERTAIN VALUES FOR THE CORNU SPIRAL

u	C(u)	S(u)
0.1	0.1000	0.0005
.2	.1999	.0042
.3	.2994	.0141
.4	.3975	.0334
.5	.4923	.0647
.6	.5811	.1105
.7	.6597	.1721
.8	.7230	.2493
.9	.7648	.3398
1.0	.7799	.4383
1.1	.7638	.5365
1.2	.7154	.6234
1.3	.6386	.6863
1.4	.5431	.7135
1.5	.4453	.6975
1.6	.3655	.6389
1.7	.3238	.5492
1.8	.3336	.4508
1.9	0.3944	0.3734

TABLE III. CALCULATIONS FOR THE HOLOGRAM PROBLEM--u_2 POSITIVE

u_2	$\mathcal{C}_2$	$\Delta\mathcal{C}$ ($\mathcal{C}_2+0.5$)	$\Delta\mathcal{C}^2$	$\mathcal{S}_2$	$\Delta\mathcal{S}$ ($\mathcal{S}_2+0.5$)	$\Delta\mathcal{S}^2$	$\Delta\mathcal{C}^2+\Delta\mathcal{S}^2$	$\sqrt{\Delta\mathcal{C}^2+\Delta\mathcal{S}^2}$	Q_o	$\Delta\mathcal{S}/\Delta\mathcal{C}$	$\tan^{-1}\frac{\Delta\mathcal{S}}{\Delta\mathcal{C}}$
0.1	0.1000	0.6000	0.360	0.0005	0.5005	0.2500	0.610	0.781	0.552	0.833	39.8
.2	.1999	.6999	.490	.0042	.5040	.2540	.744	.862	.610	.720	35.8
.3	.2994	.7990	.640	.0141	.5140	.2640	.904	.951	.672	.643	32.8
.4	.3975	.8975	.806	.0334	.5334	.2845	1.091	1.044	.738	.594	30.7
.5	.4923	.9923	.985	.0647	.5647	.3188	1.304	1.141	.806	.568	29.2
.6	.5811	1.0811	1.169	.1105	.6105	.3730	1.542	1.241	.877	.565	29.0
.7	.6957	1.1597	1.345	.1721	.6721	.4520	1.797	1.340	.947	.580	30.1
.8	.7230	1.2230	1.496	.2493	.7493	.5610	2.057	1.434	1.014	.612	31.5
.9	.7648	1.2650	1.600	.3398	.8398	.7050	2.305	1.518	1.073	.664	33.6
1.0	.7799	1.2799	1.638	.4383	.9383	.8800	2.518	1.586	1.121	.733	36.3
1.1	.7638	1.2638	1.597	.5365	1.0365	1.0740	2.671	1.634	1.155	.820	38.4
1.2	.7154	1.2154	1.478	.6234	1.1234	1.2620	2.740	1.655	1.170	.925	42.8
1.3	.6386	1.1386	1.297	.6863	1.1863	1.4070	2.704	1.644	1.162	1.042	46.2
1.4	.5431	1.0431	1.088	.7135	1.2135	1.4730	2.561	1.600	1.131	1.160	49.2
1.5	.4453	.9453	.894	.6975	1.1975	1.4340	2.328	1.525	1.078	1.265	51.7
1.6	.3655	.8655	.749	.6389	1.1389	1.2970	2.046	1.433	1.013	1.312	52.7
1.7	.3238	.8238	.679	.5492	1.0492	1.101	1.780	1.334	.943	1.271	51.8
1.8	.3336	.8336	.6950	.4508	.9508	.9040	1.599	1.264	.893	1.140	48.8
1.9	0.3944	0.8944	0.8000	0.3734	0.8734	0.7630	1.563	1.250	0.884	0.997	44.4

TABLE III (continued). CALCULATIONS FOR THE HOLOGRAM PROBLEM--u_2 POSITIVE

$45°-\tan^{-1}\sqrt{45+\Delta\Gamma}$	$\Psi/2$	a_o	$6a_o$	a_o^2	$9+a_o^2$	I_{max}	I_{min}	CONTRAST	u_2
5.2	0.0423	0.552	3.312	0.304	9.304	12.616	5.992	0.356	0.1
9.2	.0748	.610	3.660	.372	9.372	13.032	5.712	.390	.2
12.2	.0992	.672	4.032	.690	9.452	14.680	4.700	.426	.3
14.3	.1162	.738	4.428	.545	9.545	13.973	5.117	.463	.4
15.8	.1285	.806	4.836	.649	9.649	14.485	4.813	.501	.5
16.0	.1301	.877	5.262	.769	9.769	15.031	4.507	.538	.6
14.9	.1211	.947	5.682	.896	9.896	15.578	4.214	.574	.7
13.5	.1098	1.014	6.084	1.028	10.028	16.112	3.944	.606	.8
11.4	.0927	1.073	6.438	1.151	10.151	16.589	3.713	.634	.9
8.7	.0707	1.121	6.726	1.256	10.256	16.982	3.530	.655	1.0
6.6	.0537	1.155	6.930	1.334	10.334	17.264	3.404	.670	1.1
2.2	.0179	1.170	7.020	1.368	10.368	17.388	3.348	.667	1.2
-1.2	-.0096	1.162	6.972	1.350	10.350	17.322	3.378	.673	1.3
-4.2	-.0341	1.131	6.786	1.279	10.279	17.065	3.493	.660	1.4
-6.7	-.0545	1.078	6.468	1.162	10.162	16.630	3.694	.636	1.5
-7.7	-.0626	1.013	6.078	1.026	10.026	16.104	3.948	.606	1.6
-6.8	-.0551	.943	5.568	.889	9.889	15.547	4.231	.572	1.7
-3.8	-.0309	.893	5.358	.797	9.797	15.155	4.439	.546	1.8
0.6	0.0049	0.884	5.304	0.781	9.781	15.085	4.477	0.542	1.9

TABLE IV CALCULATIONS FOR THE HOLOGRAM PROBLEM--u_2 NEGATIVE

u_2	$\Delta\zeta$	$\Delta\zeta^2$	$\Delta\xi$	$\Delta\xi^2$	$\Delta\zeta^2+\Delta\xi^2$	$\sqrt{\Delta\zeta^2+\Delta\xi^2}$	a_0	$\Delta\xi/\Delta\zeta$	$\tan^{-1}\frac{\Delta\xi}{\Delta\zeta}$
-0.1	0.4000	0.1600	0.4995	0.2500	0.4100	0.6400	0.5430	1.299	51.2
-.2	..3001	.0900	.4958	.2458	.3358	.5794	.4097	1.652	58.8
-.3	..2006	.0902	.4859	.2360	.2762	.5255	.3716	2.422	67.6
-.4	.1035	.0105	.4966	.2466	.2571	.5070	.3585	4.845	78.3
-.5	.0077	.0000	.4353	.1894	.4853	.3078	.3078	56.532	90.0
-.6	-.0811	.0065	.3895	.1517	.1582	.3977	.2812	-4.803	102.0
-.7	-.1597	.0255	.3279	.1075	.1330	.3646	.2587	-2.053	116.0
-.8	-.2228	.0496	.2507	.0628	.1124	.3352	.2370	-1.125	131.9
-.9	-.2648	.0701	.1602	.0256	.0957	.3093	.2187	-0.605	148.8
-1.0	-.2799	.0783	.0617	.0038	.0821	.2865	.2026	-.2204	167.6
-1.1	-.2638	.0695	-.0365	.0013	.0708	.2660	.1881	.1383	187.9
-1.2	-.2154	.0463	-.1234	.0152	.0615	.2479	.1753	.5728	209.8
-1.3	-.1368	.0192	-.1863	.0347	.0539	.2321	.1641	1.3441	233.4
-1.4	-.0430	.0019	-.2135	.0455	.0474	.2180	.1540	4.9700	258.6
-1.5	.0547	.0030	-.1975	.0390	.0420	.2050	.1450	-3.6100	285.5
-1.6	.1345	.0180	-.1389	.0192	.0372	.1928	.1363	-1.0330	314.0
-1.7	.1762	.0310	-.0492	.0024	.0334	.1827	.1292	-0.2792	344.4
-1.8	.1663	.0276	.0491	.0024	.0300	.1732	.1224	.2952	376.4
-1.9	0.1055	0.0111	0.1266	0.0160	0.0271	0.1646	0.1164	0.2000	410.2

TABLE IV (continued). CALCULATIONS FOR THE HOLOGRAM PROBLEM--u_2 NEGATIVE

$45^\circ - \tan^{-1}\sqrt{\Delta\xi^2+\Delta\zeta^2}$	ψ/λ	a_0	$6a_0$	a_0^2	$9+a_0^2$	I_{max}	I_{min}	CONTRAST	u_2
-6.2	-0.0504	0.4530	2.718	0.2050	9.2050	11.923	6.487	0.295	-0.1
-13.8	-.1121	.4097	2.458	.1678	9.1678	11.398	6.710	.268	-.2
-22.6	-.1837	.3716	2.230	.1380	9.1380	11.368	6.908	.244	-.3
-33.3	-.2707	.3585	2.151	.1285	9.1285	11.280	6.978	.236	-.4
-45.0	-.3660	.3078	1.847	.0947	9.0947	10.942	7.248	.203	-.5
-57.0	-.4630	.2812	1.687	.0790	9.0790	10.766	7.392	.186	-.6
-71.0	-.5770	.2578	1.547	.0664	9.0664	10.613	7.519	.171	-.7
-86.9	-.7070	.2370	1.422	.0561	9.0561	10.478	7.634	.157	-.8
-103.8	-.8440	.2187	1.3122	.0478	9.0478	10.360	7.736	.145	-.9
-122.6	-.997	.2026	1.216	.0410	9.0410	10.257	7.825	.134	-1.0
-142.9	-1.162	.1881	1.129	.0353	9.0353	10.164	7.906	.125	-1.1
-164.8	-1.340	.1753	1.052	.0307	9.0307	10.083	7.979	.116	-1.2
-184.4	-1.532	.1641	.9845	.0269	9.0269	10.012	8.042	.109	-1.3
-213.6	-1.737	.1540	.9240	.0237	9.0237	9.948	8.100	.102	-1.4
-240.5	-1.955	.1450	.8700	.0210	9.0210	9.891	8.151	.096	-1.5
-269.0	-2.190	.1363	.8180	.0185	9.0185	9.837	8.201	.091	-1.6
-299.4	-2.434	.1242	.7450	.0154	9.0154	9.760	8.270	.0826	-1.7
-351.4	-2.694	.1224	.7340	.0149	9.0149	9.749	8.281	.0814	-1.8
-365.2	-2.970	0.1164	0.6980	0.0135	9.0135	9.712	8.316	0.0774	-1.9

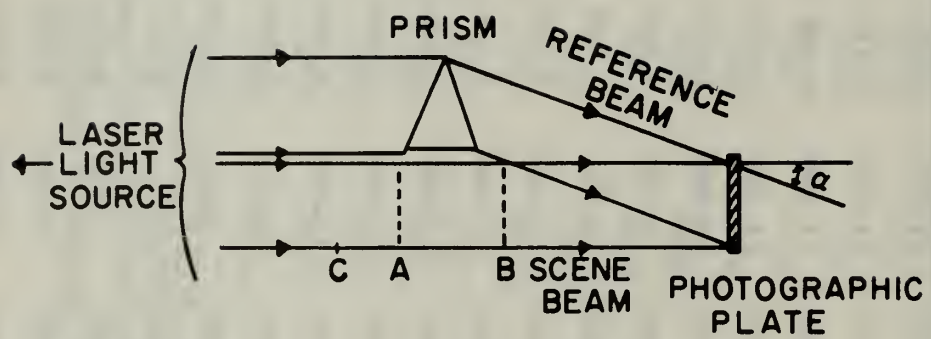

Figure Ia. Exposure of the Hologram.

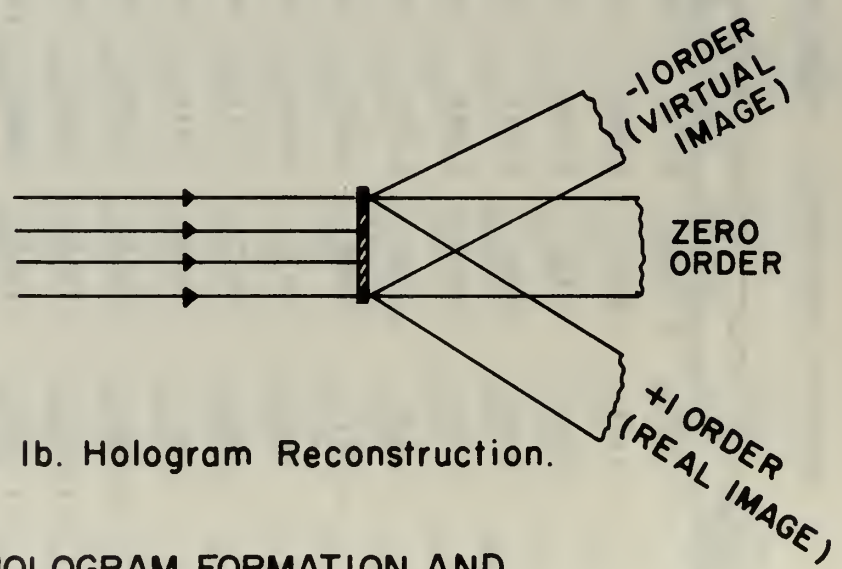

Figure Ib. Hologram Reconstruction.

Figure I HOLOGRAM FORMATION AND RECONSTRUCTION.

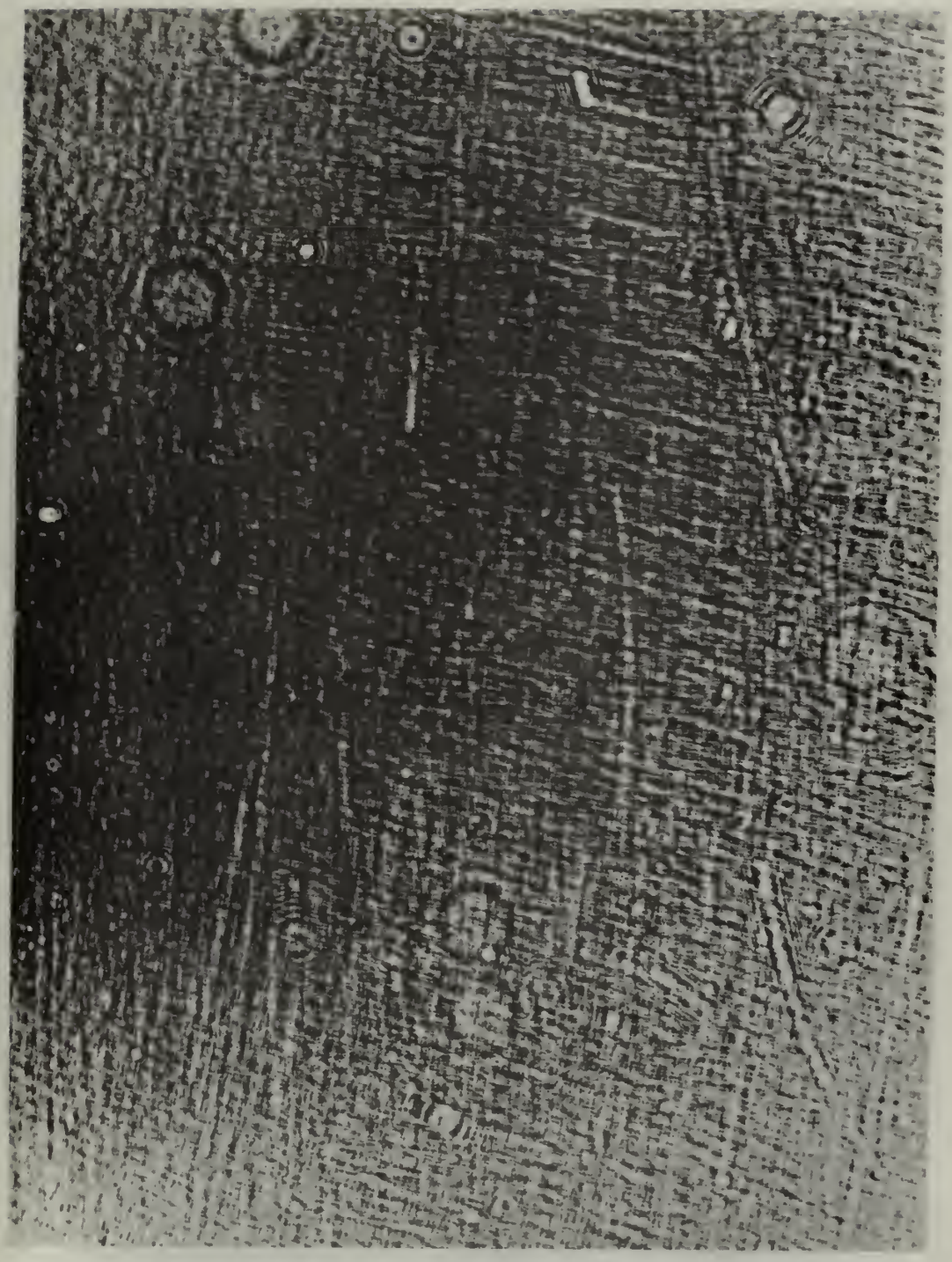

Figure 2 PHOTOGRAPH OF A LIGHT-FIELD HOLOGRAM

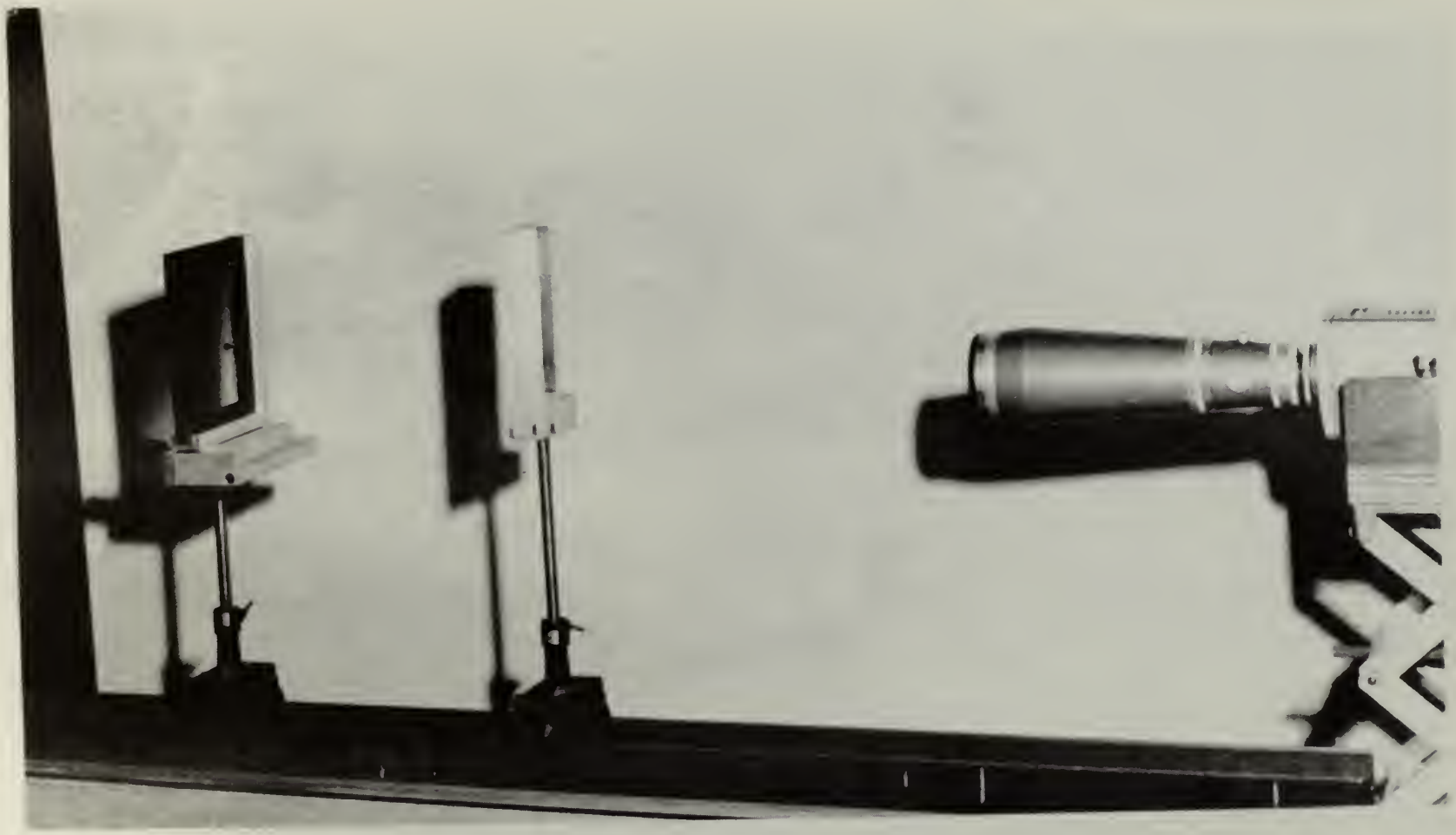

Figure 3 PHOTOGRAPH OF APPARATUS USED FOR CONSTRUCTING HOLOGRAMS

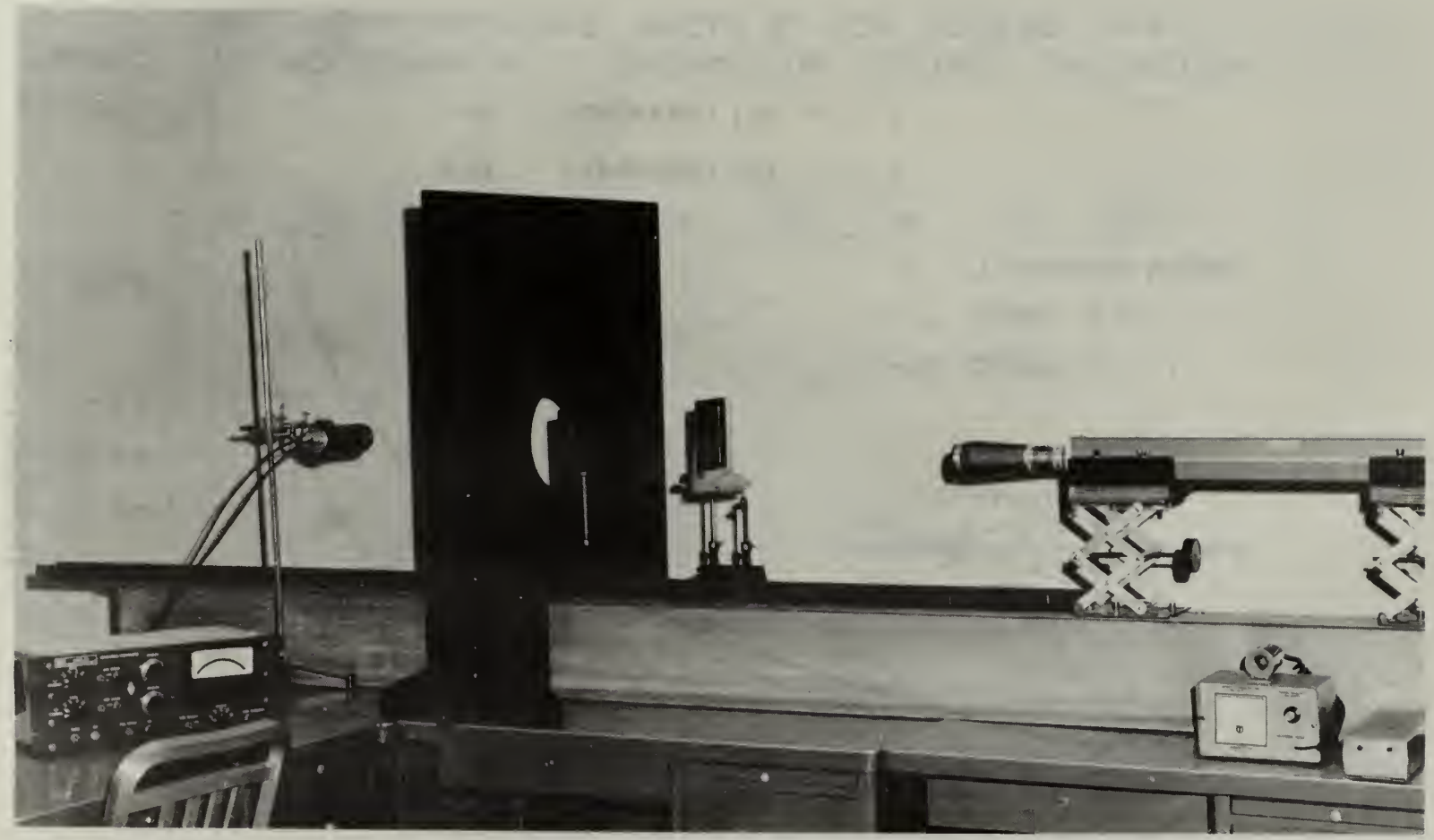

Figure 4 PHOTOGRAPH OF APPARATUS USED FOR MAKING INTENSITY MEASUREMENTS

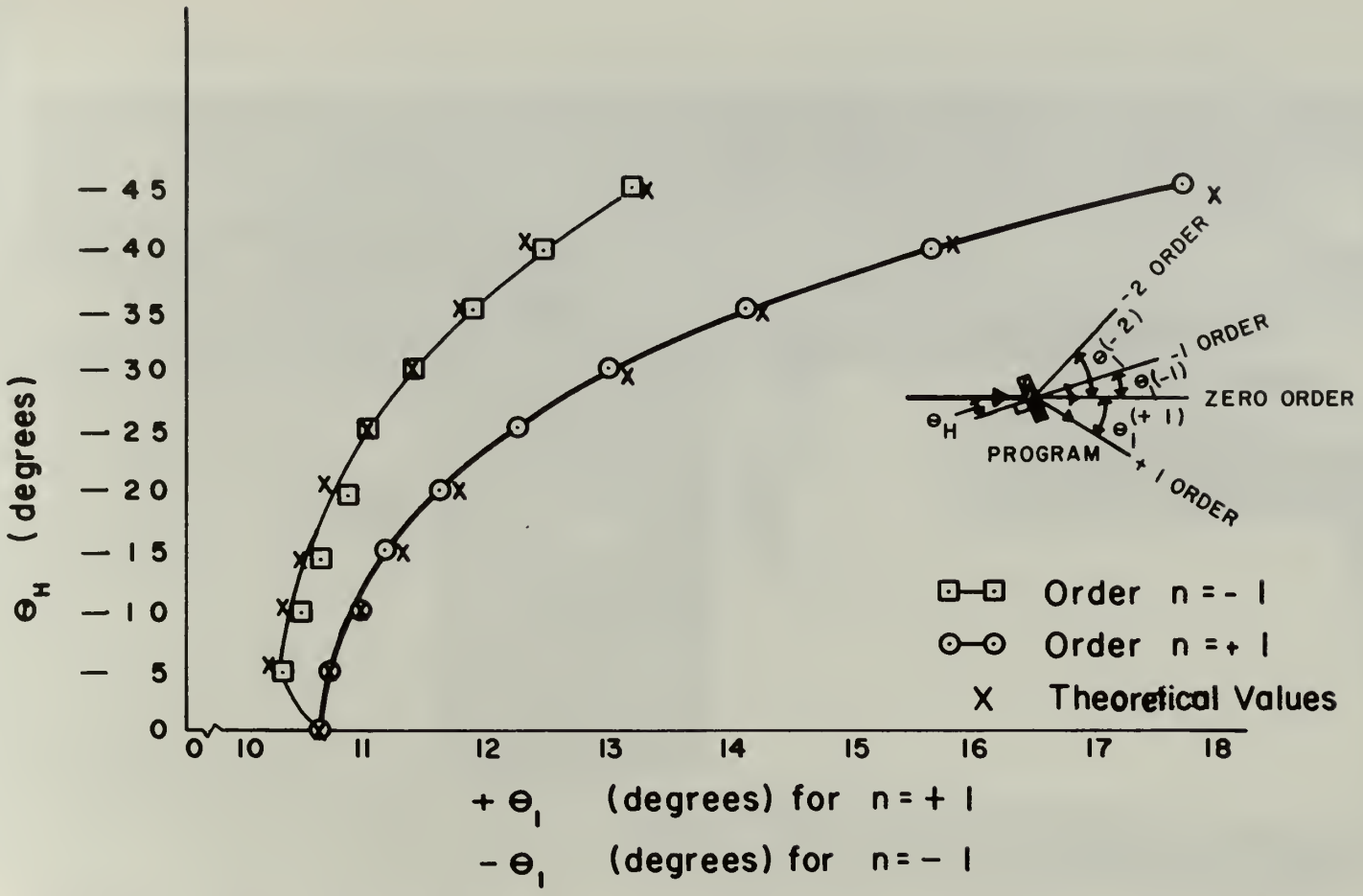

Figure 5 THE HOLOGRAM AS A DIFFRACTION GRATING, DIFFRACTION ANGLE θ_1 vs. INCIDENCE ANGLE θ_H FOR ORDERS n = ±1

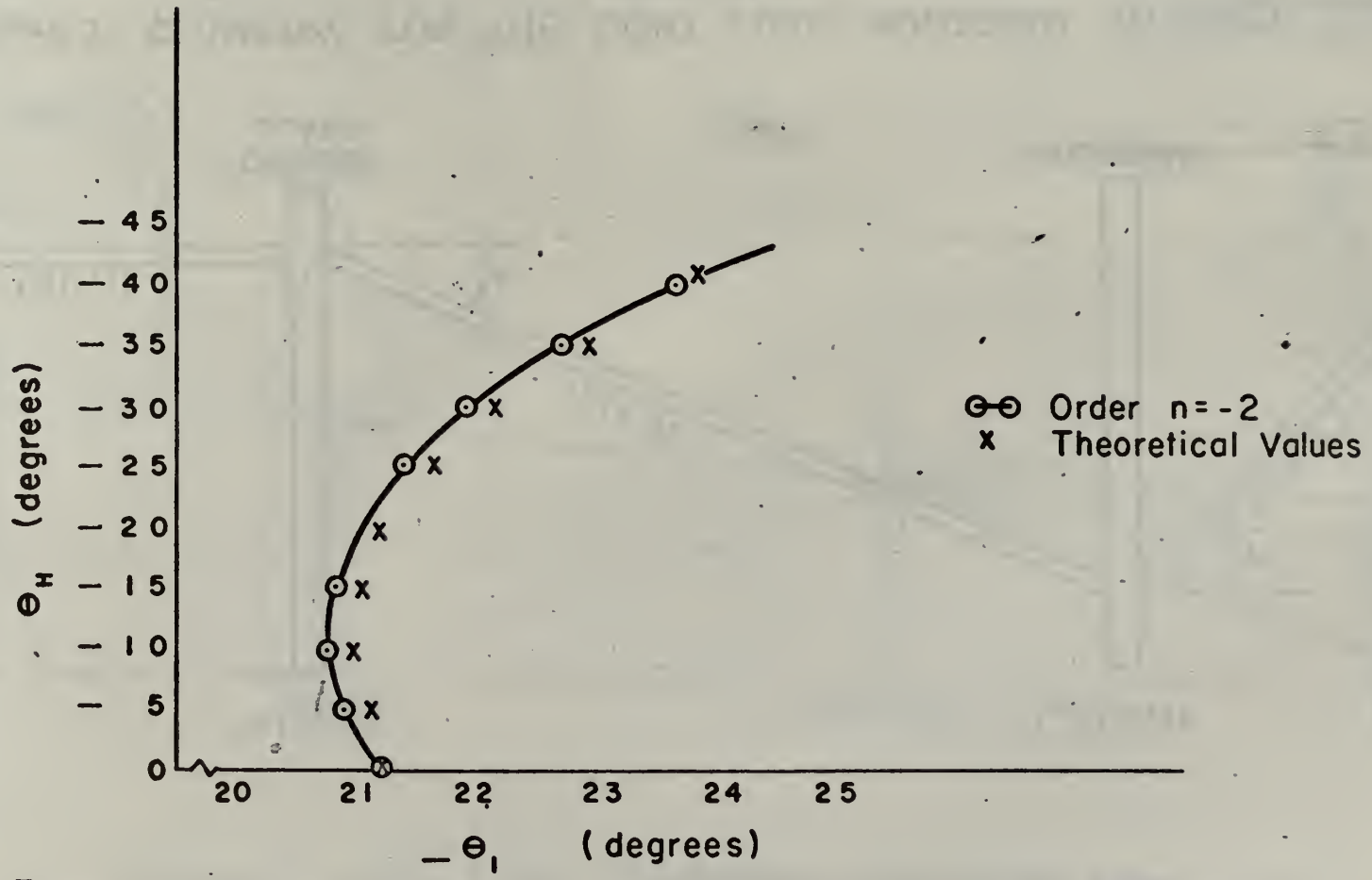

Figure 6 THE HOLOGRAM AS A DIFFRACTION GRATING, DIFFRACTION ANGLE θ_1 vs. INCIDENCE ANGLE θ_H FOR ORDER n=-2

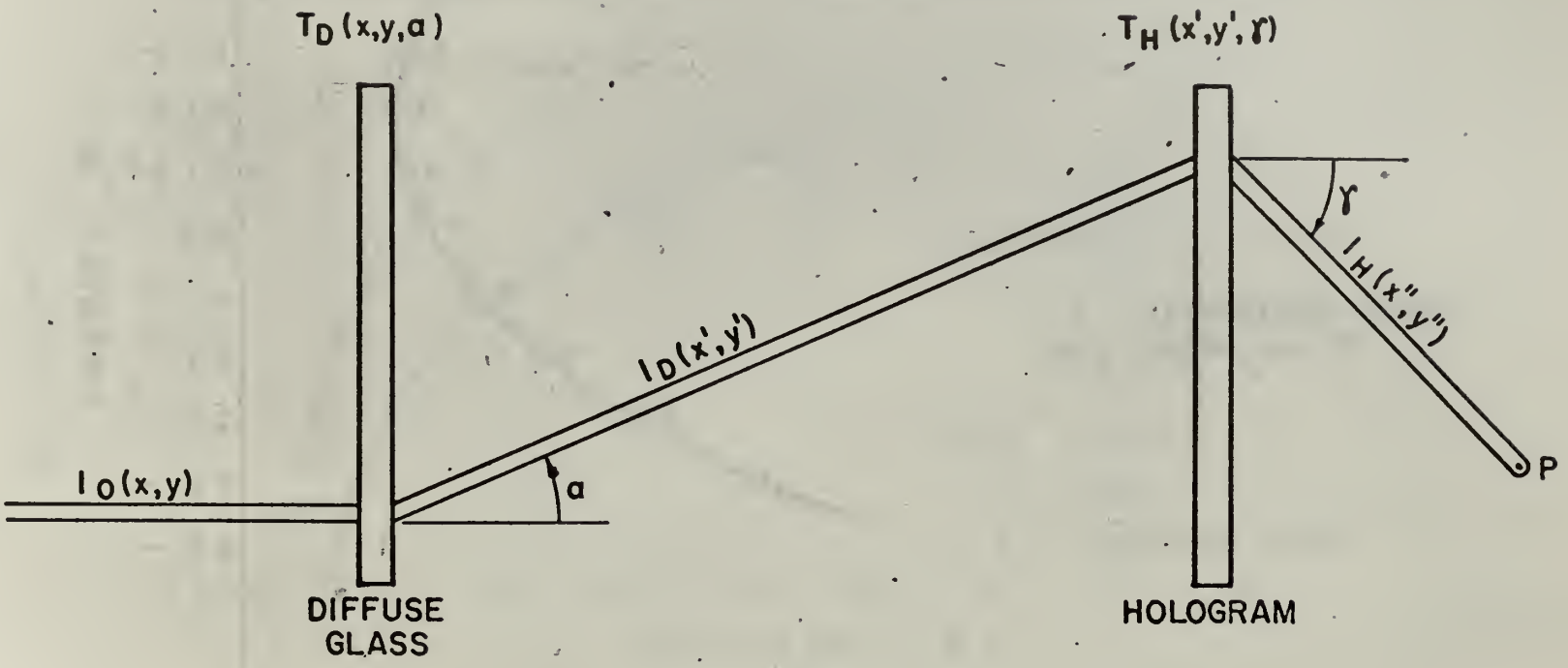

Figure 7 GEOMETRY FOR THE LIGHT-FIELD HOLOGRAM INTENSITY PROBLEM

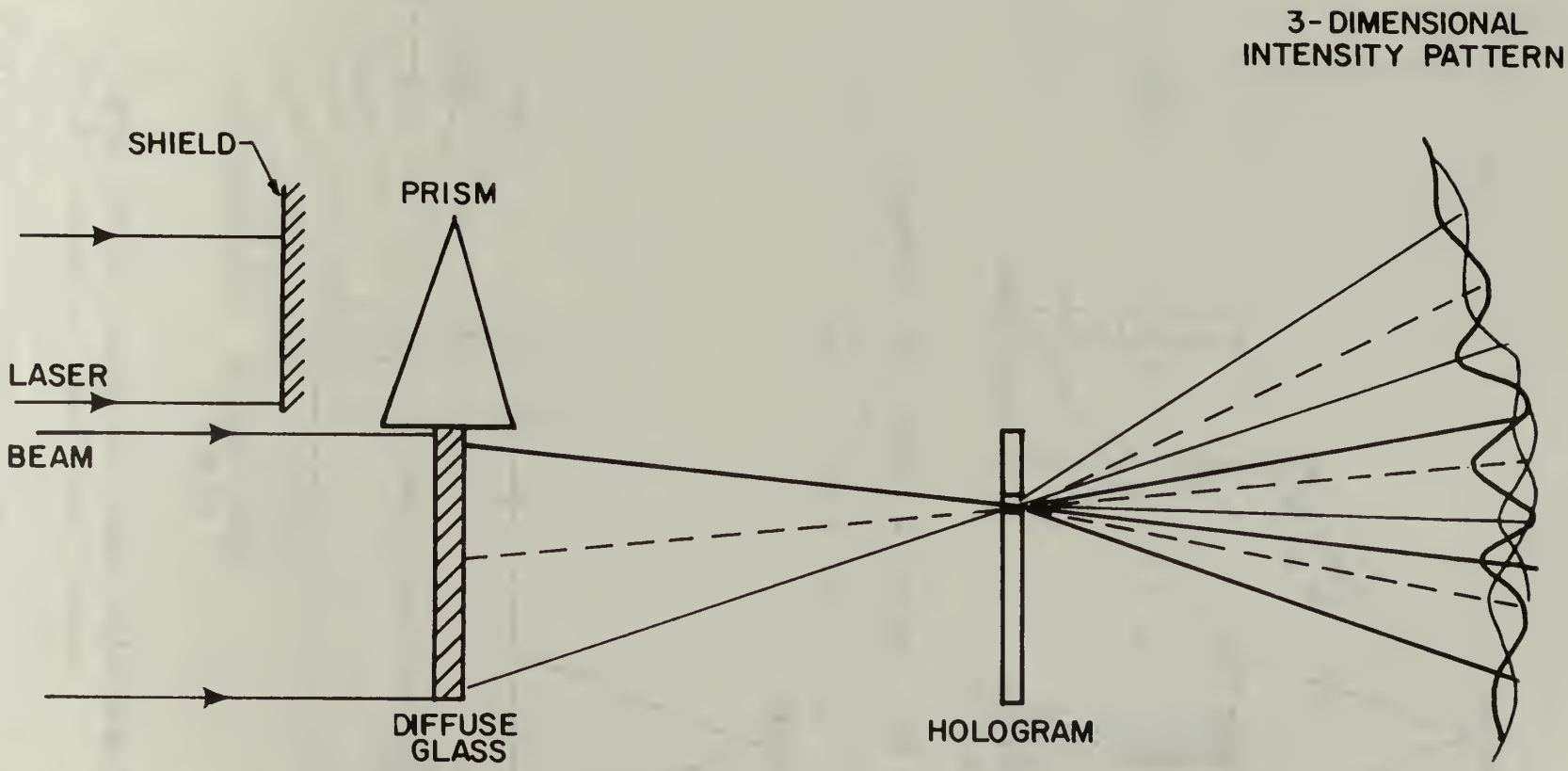

Figure 8 LIGHT-FIELD HOLOGRAM RECONSTRUCTION

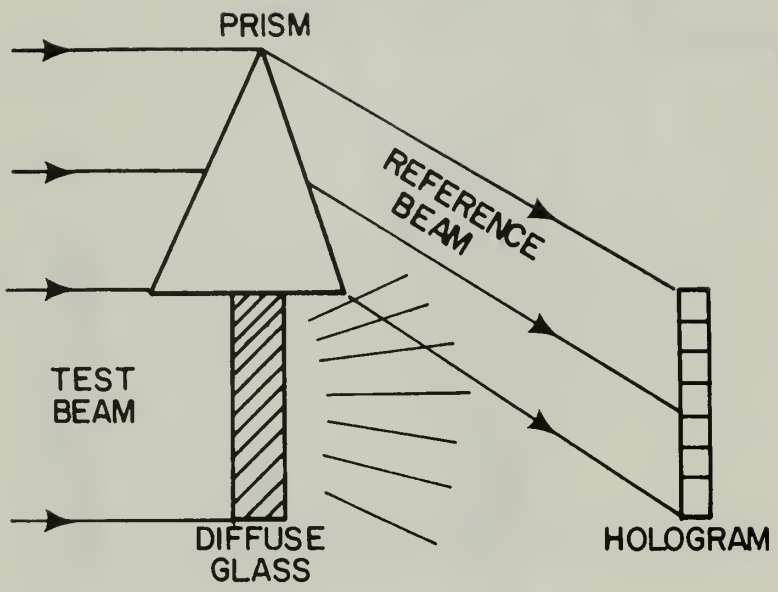

Figure 9a Making A Light-Field Hologram

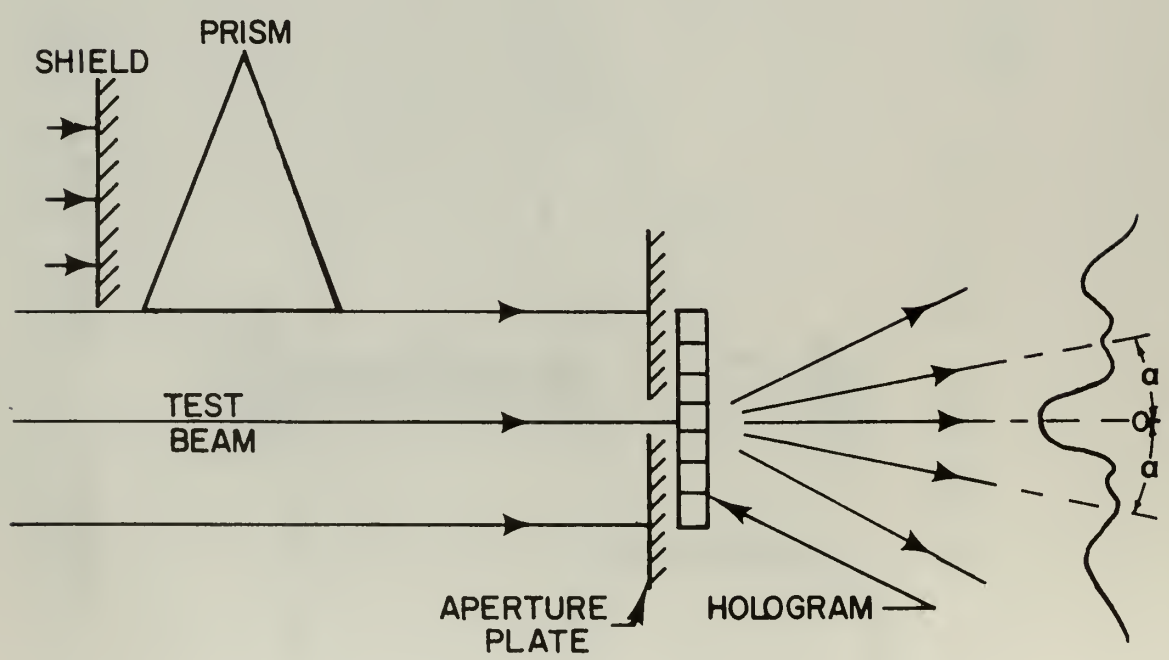

Figure 9b Light-Field Hologram Reconstruction At Normal Test Beam Incidence ($\theta_H = 0$)

Figure 9 EXPOSURE AND INTENSITY DISTRIBUTION OF A LIGHT-FIELD HOLOGRAM

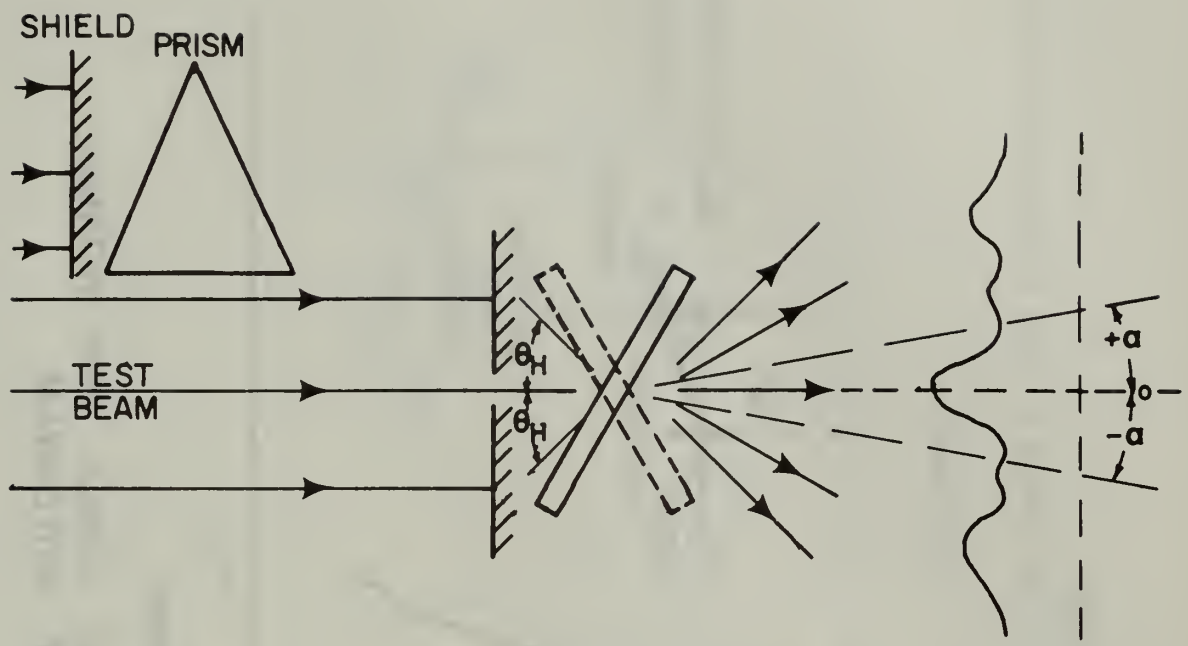

Figure 10a Light-Field Hologram Reconstruction With Test Beam Incidence Angle $\pm\theta_H$

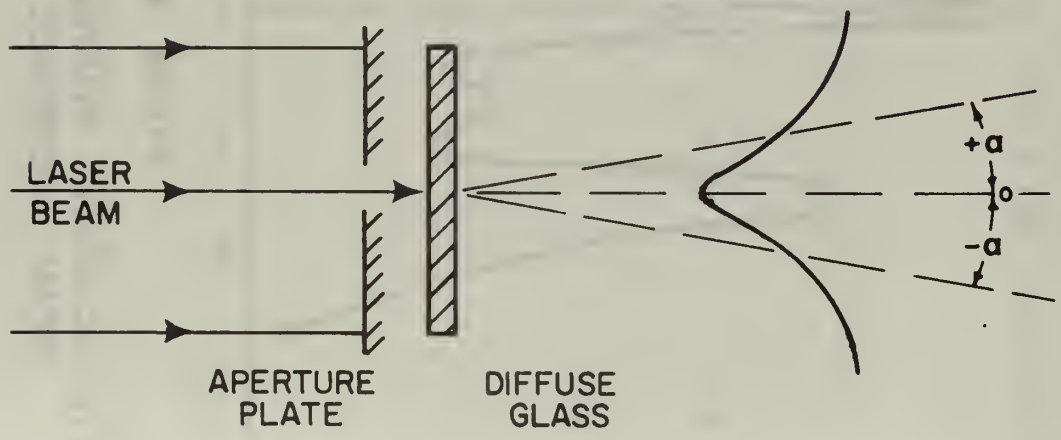

Figure 10b Intensity Distribution of Diffuse Glass

Figure 10 INTENSITY DISTRIBUTION OF A LIGHT-FIELD HOLOGRAM AND OF DIFFUSE GLASS

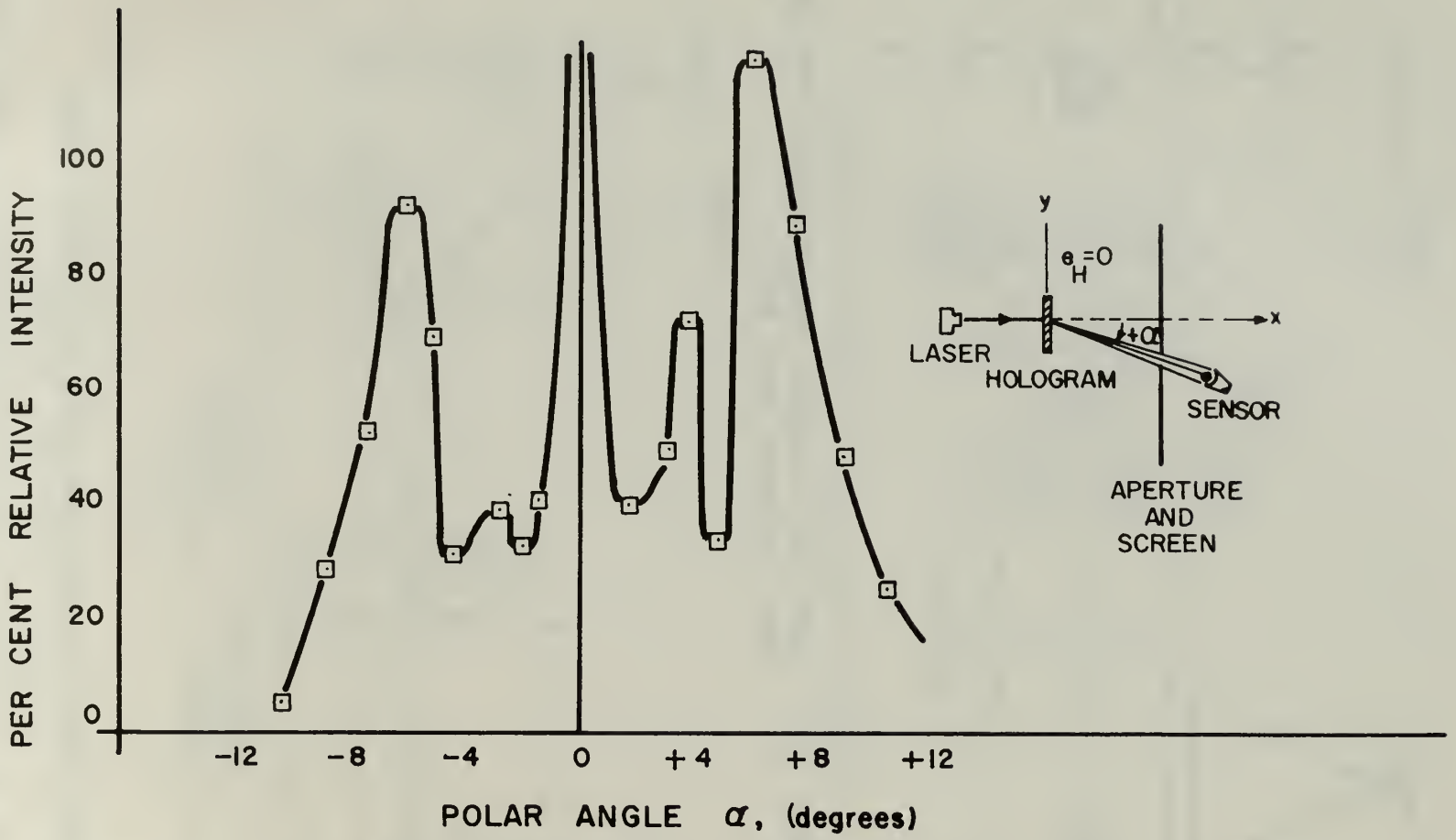

Figure 11 RELATIVE INTENSITY vs. POLAR ANGLE FOR NORMAL BEAM INCIDENCE ON DIFFUSE HOLOGRAM

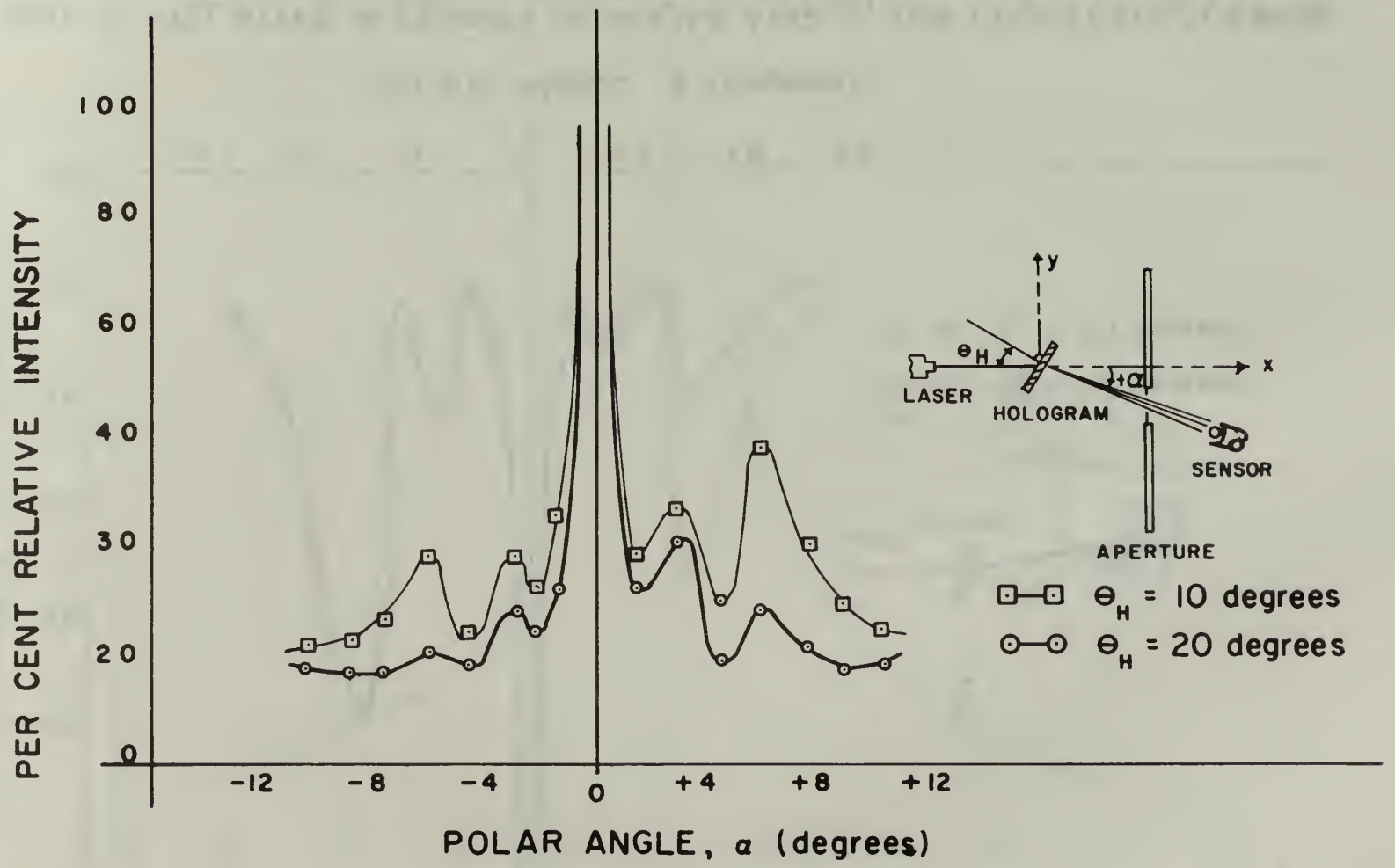

Figure 12 RELATIVE INTENSITY vs. POLAR ANGLE FOR CLOCKWISE ROTATION OF DIFFUSE GLASS HOLOGRAM.

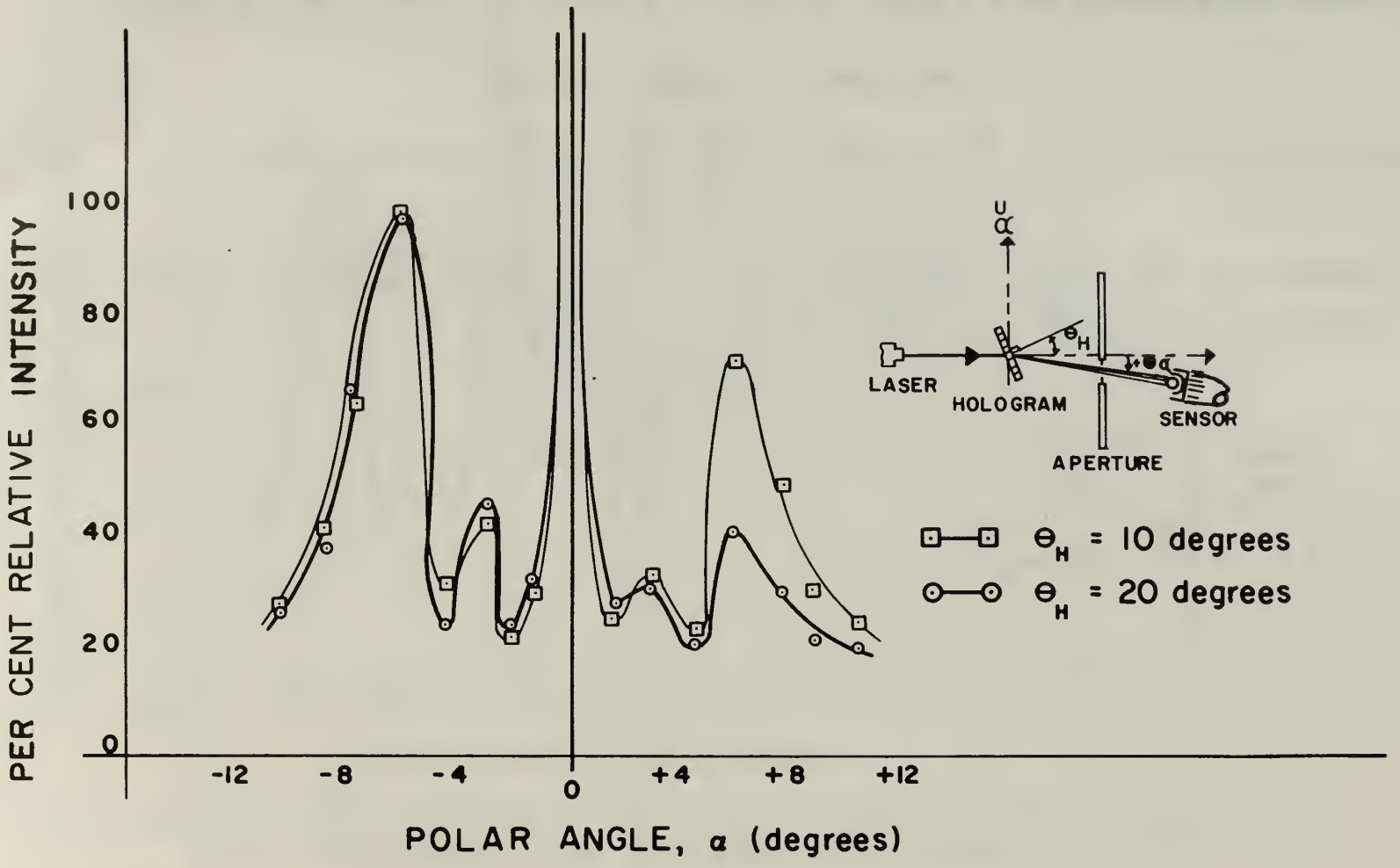

Figure 13 RELATIVE INTENSITY vs. POLAR ANGLE, FOR COUNTERCLOCKWISE ROTATION OF DIFFUSE GLASS HOLOGRAM.

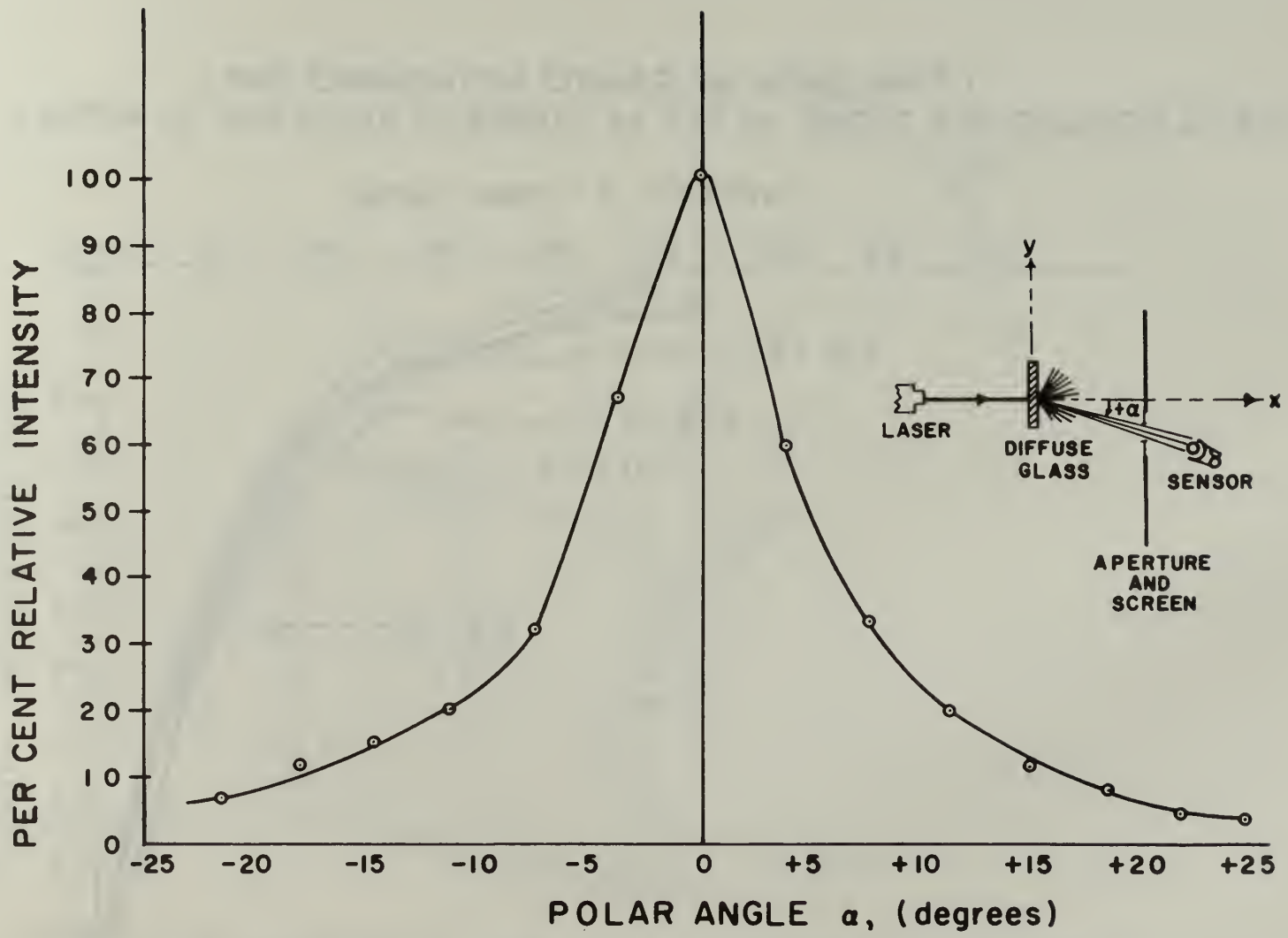

Figure 14 RELATIVE INTENSITY vs. POLAR ANGLE FOR NORMAL BEAM INCIDENCE ON DIFFUSE GLASS.

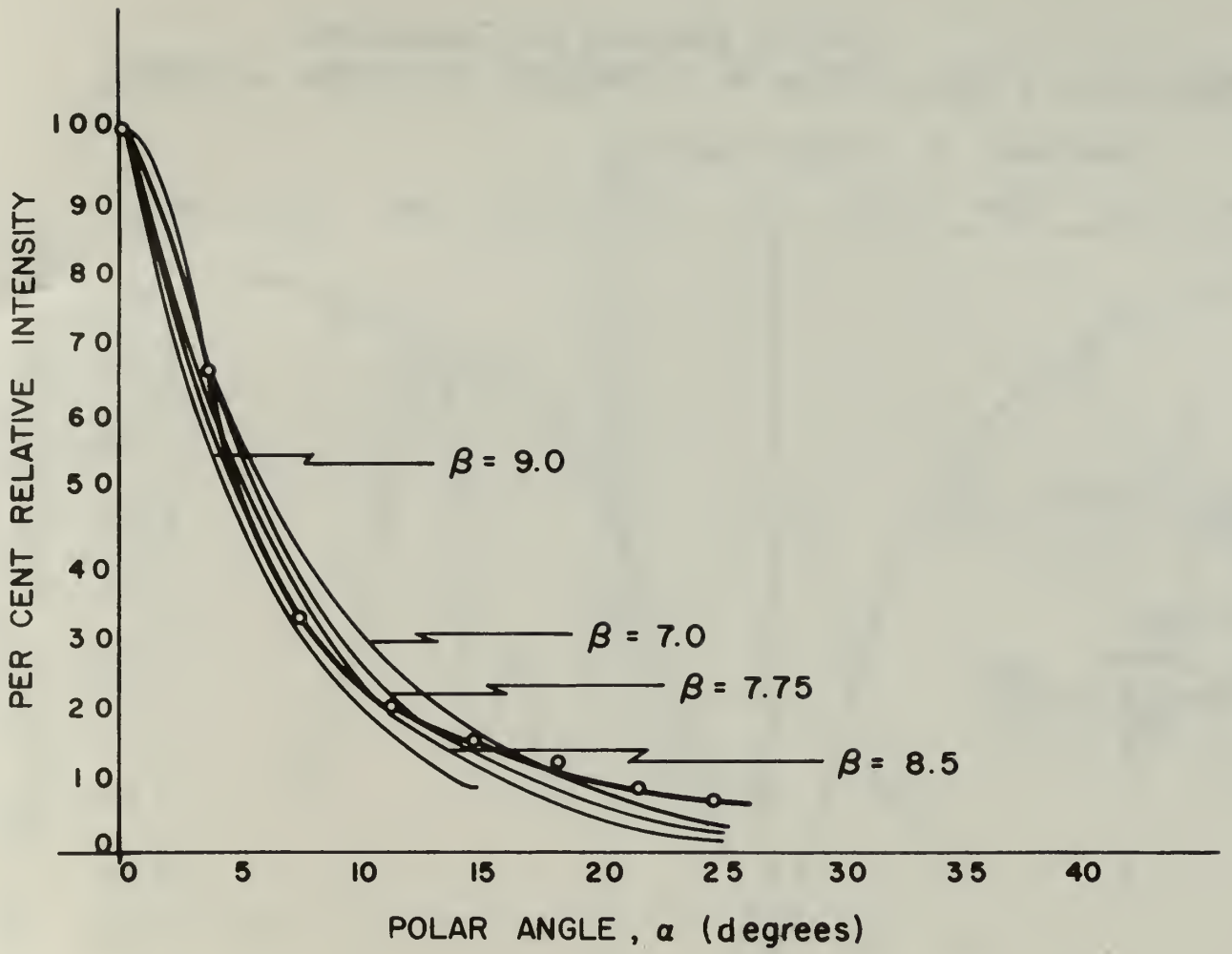

Figure 15 RELATIVE INTENSITY vs. POLAR ANGLE FOR DIFFUSE GLASS AND COMPARISON CURVES OF $\exp(-\beta \tan \alpha)$

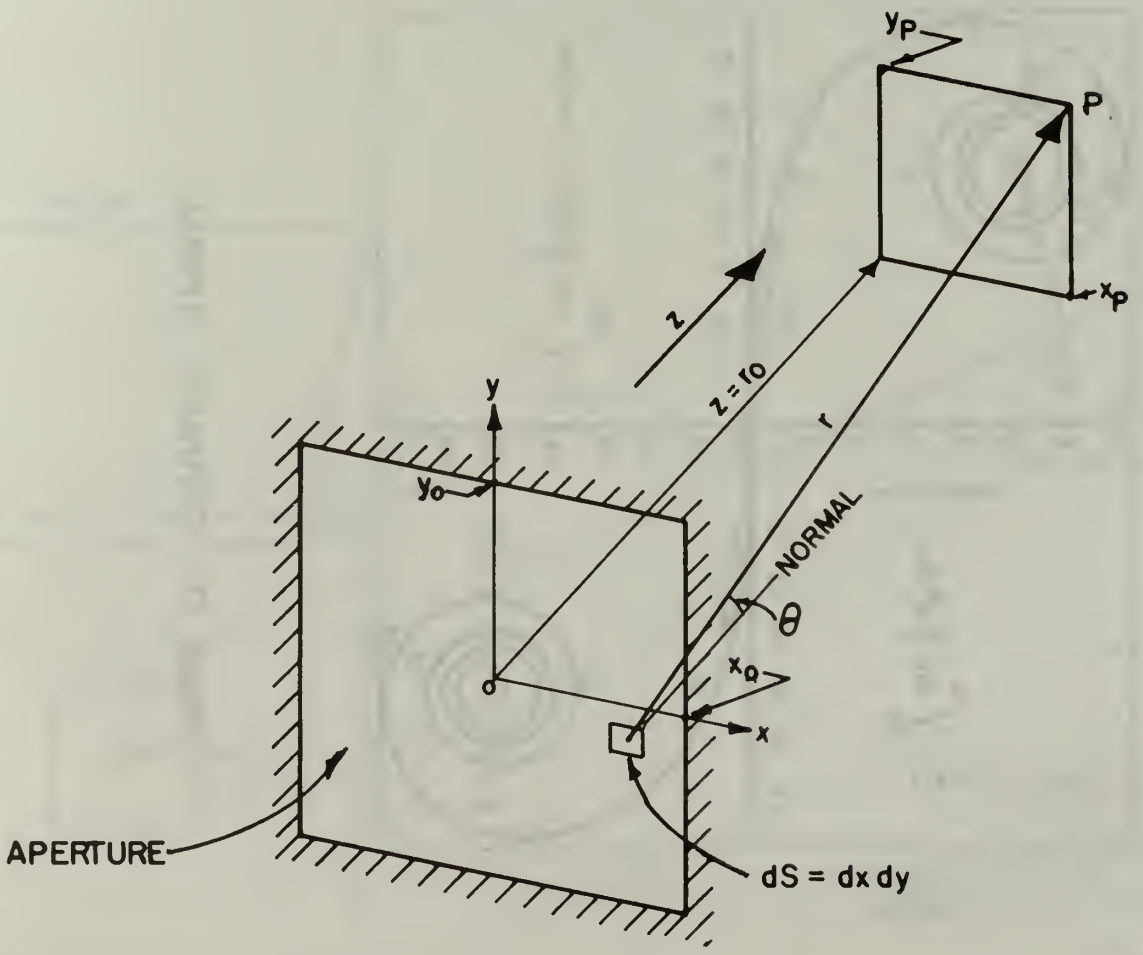

Figure 16 GEOMETRY FOR THE KIRCHHOFF DIFFERENTIAL

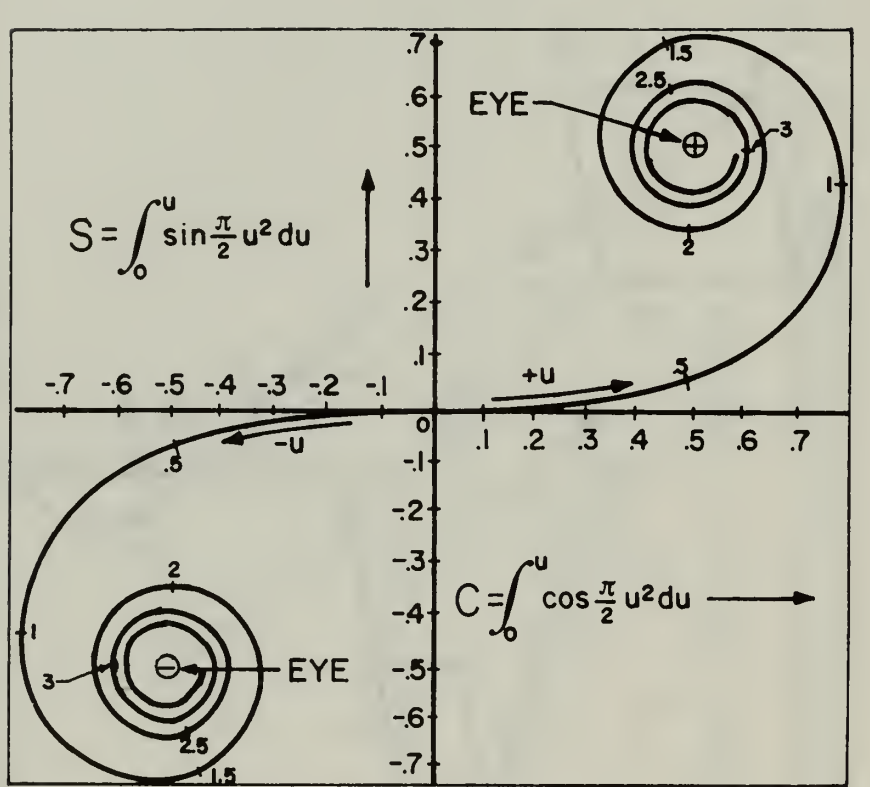

Figure 17 CORNU'S SPIRAL

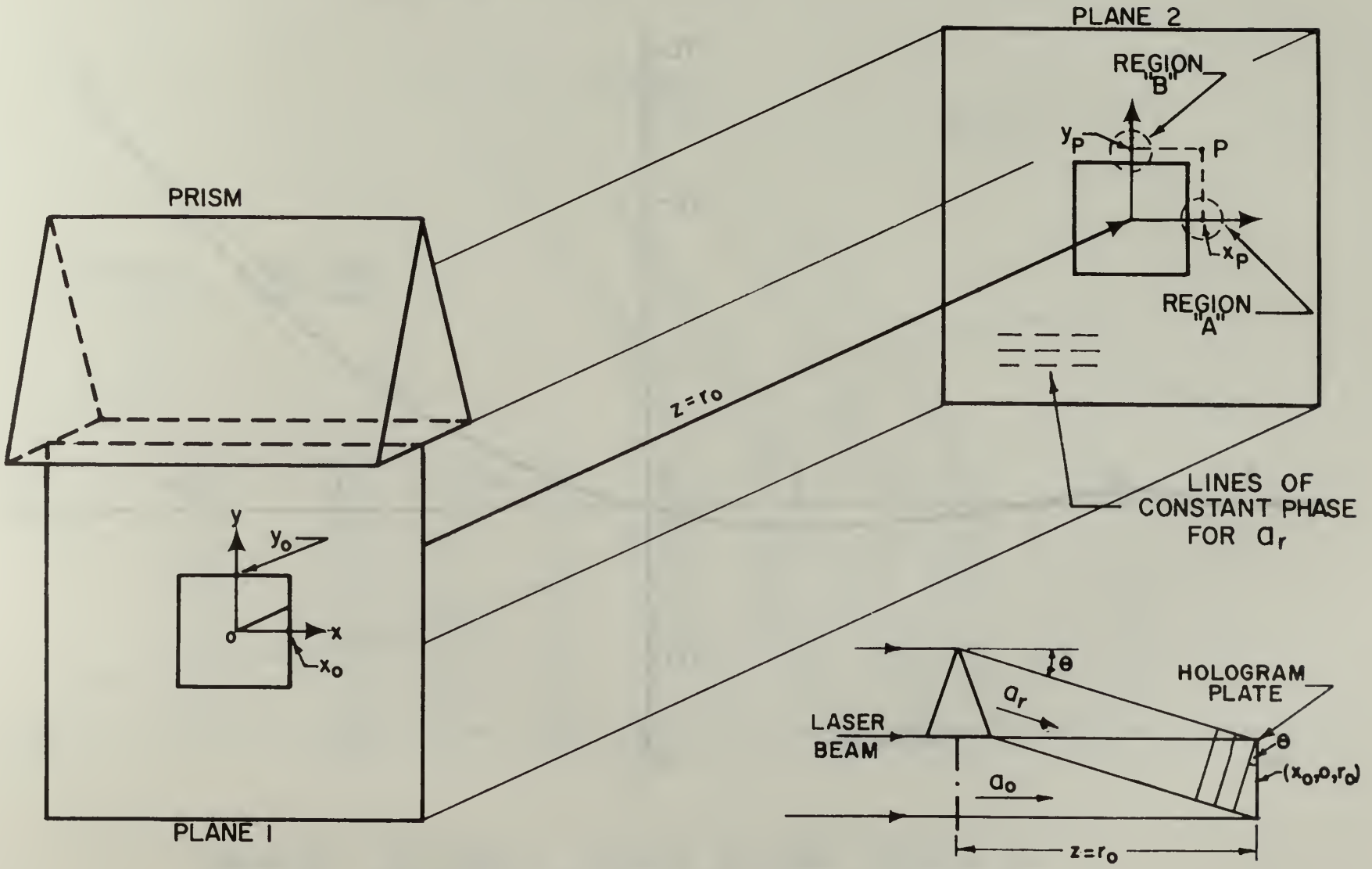

Figure 18 GEOMETRY OF THE HOLOGRAM PROBLEM

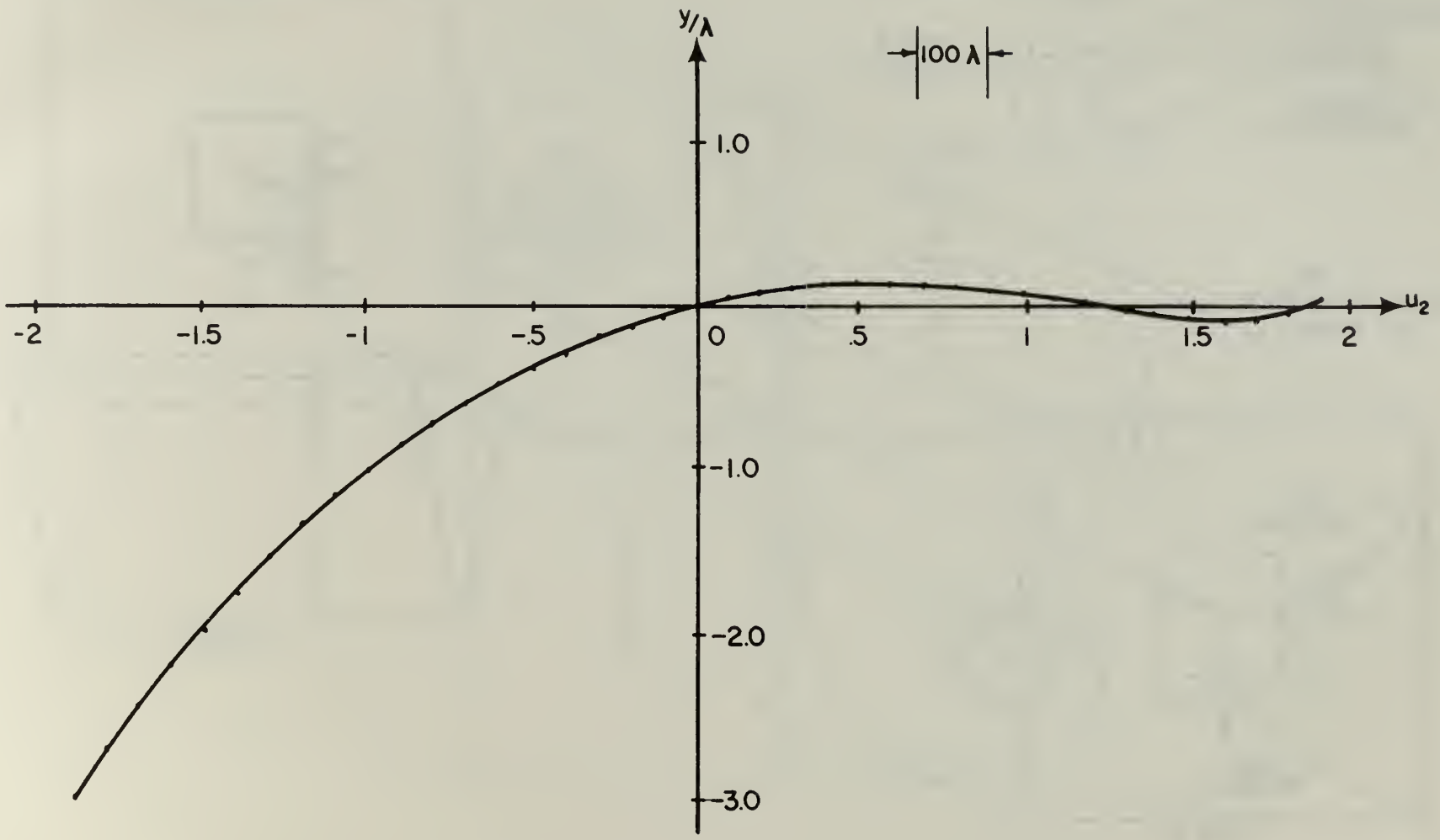

Figure 19 LOCI OF INTENSITY MAXIMA IN REGION "A"

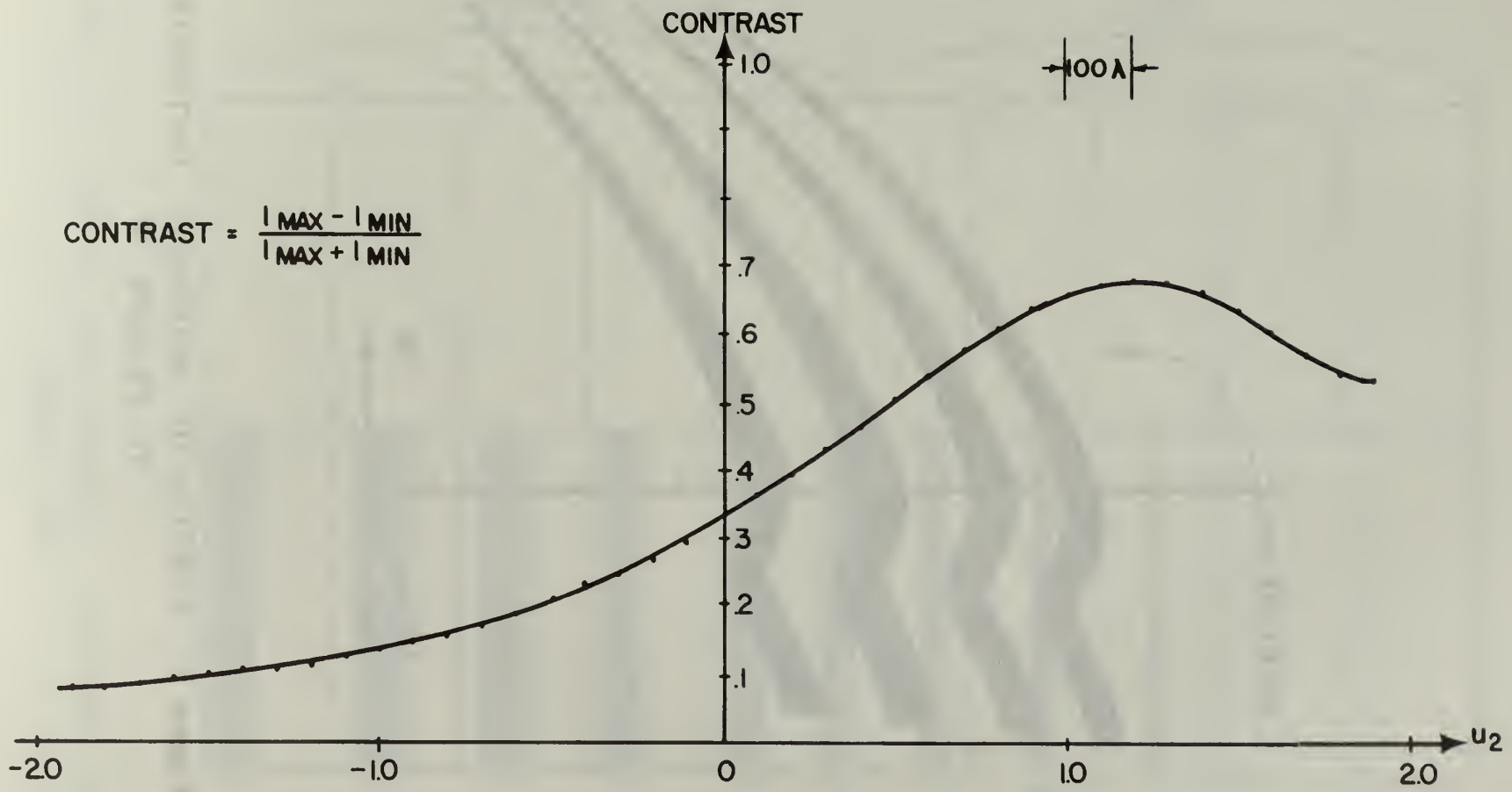

Figure 20 CONTRAST - REGION "A" AND REGION "B"

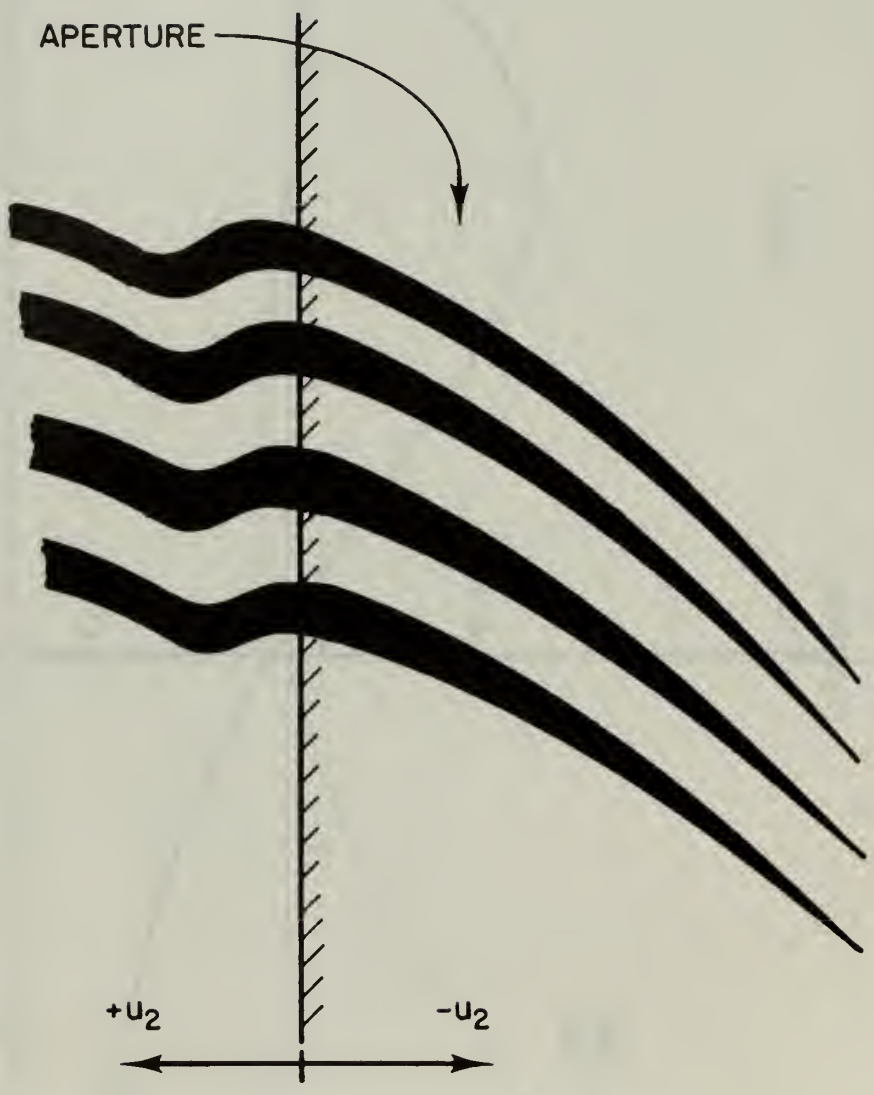

Figure 21 SKETCH OF INTENSITY DISTRIBUTION IN REGION "A"

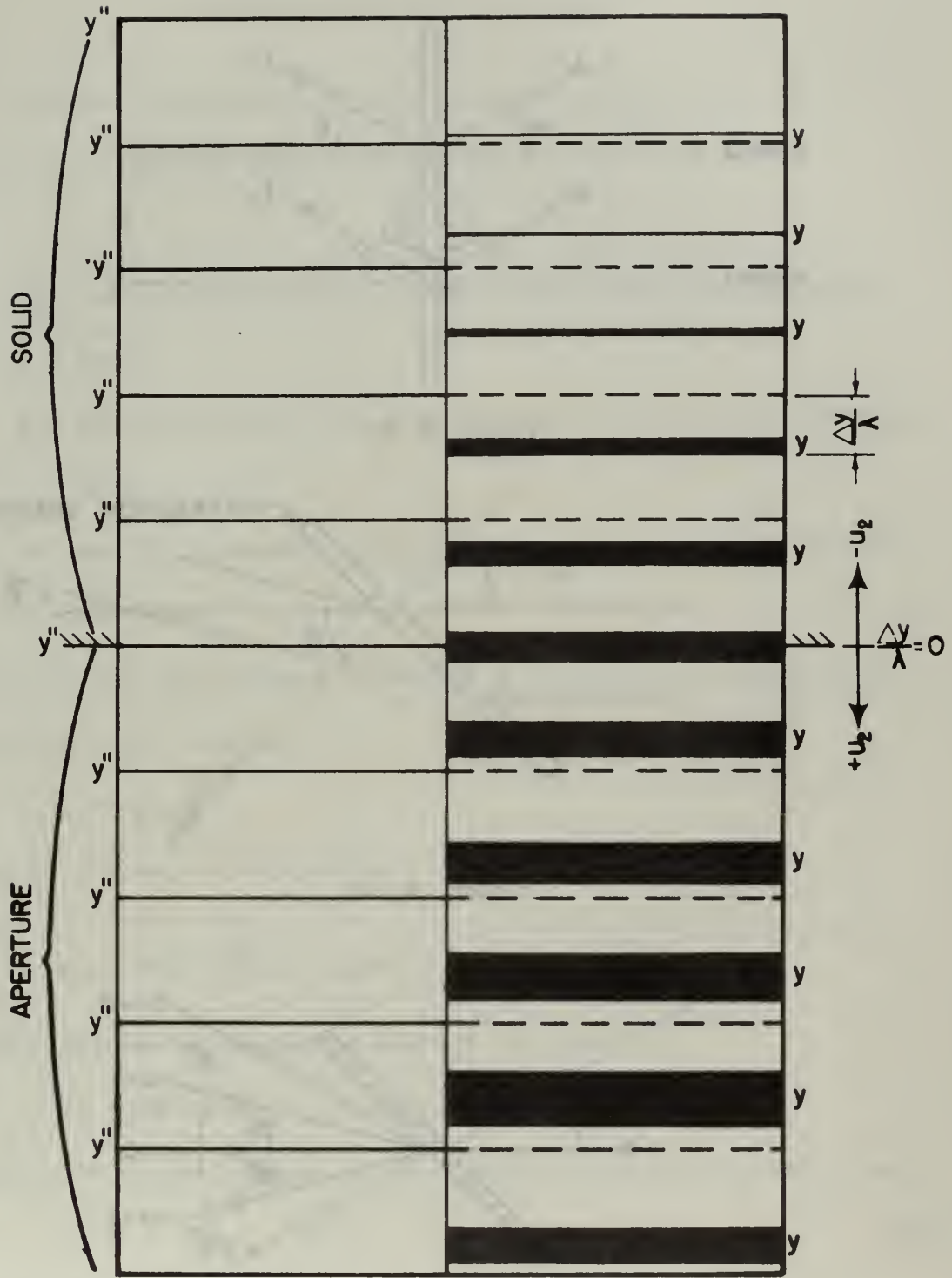

Figure 22 SKETCH OF INTENSITY DISTRIBUTION IN REGION "B"

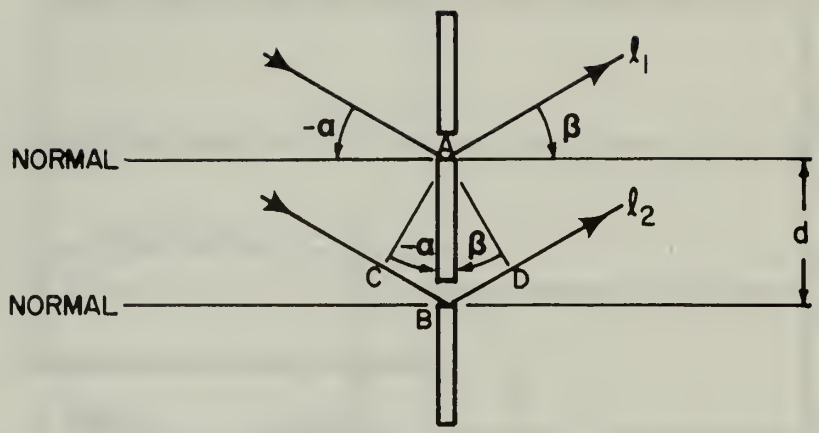

Figure A Ia

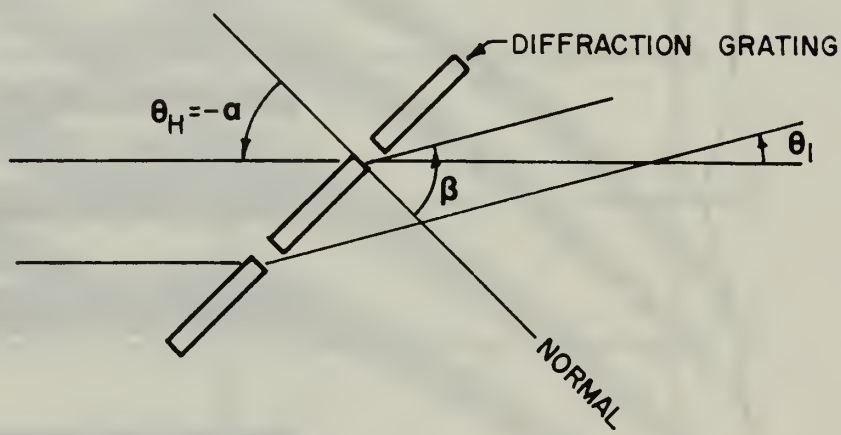

Figure A Ib

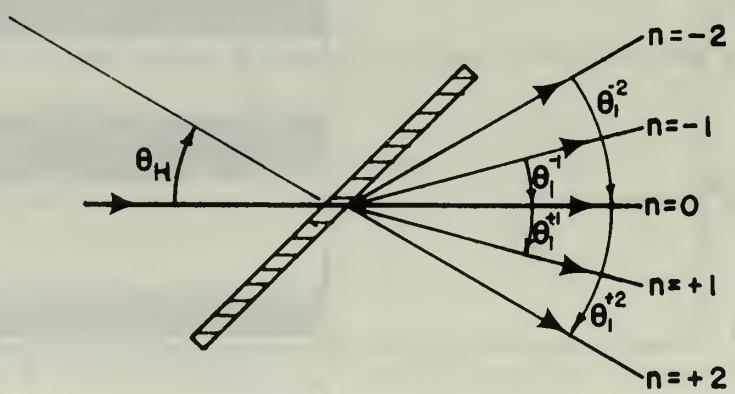

Figure A Ic

Figure A I PROPERTIES OF THE DIFFRACTION GRATING

APPENDIX

DIFFRACTION GRATING THEORY[21]

Consider a plane beam of light which is incident upon a lined diffraction grating as shown in Figure A1a.

Let:

α = the angle between the normal to the grating and the incident beam

β = the angle between the normal to the grating and the diffracted beam

α and β be measured positive in the clockwise direction from the normal.

It can be seen from Figure A1a that ray ℓ (2) must travel further than ray ℓ (1) by the distance

CB + BD.

From the geometry of Figure A1a:

$$\sin(-\alpha) = \frac{CB}{AB} = -\sin\alpha \quad ; \quad \sin\beta = \frac{BD}{AB}$$

If AB is defined as the grating spacing, d, and if

$$BD - CB = n\lambda \qquad n = 0, \pm 1, \pm 2, \ldots\ldots$$

which is an integral number of wavelengths of the incident light, then

$$\sin\beta - \sin\alpha = \frac{n\lambda}{d} \tag{A1}$$

where n is negative for $\alpha > \beta$ in absolute value.

The successive images formed for n = 0, $\pm$ 1, $\pm$ 2, etc., are called images of the zero order, first order, second order, and so on.

For zero angle of incidence

$$\alpha = 0$$

and the grating spacing is given by

$$d = \frac{n\lambda}{\sin \beta}$$

Instead of having the beam incident upon a vertical grating at an angle α, let the incident be kept horizontal and the diffraction grating be rotated about a horizontal axis by the amount α as shown in Figure A1b.

Define:

$$\theta_H \equiv -\alpha$$

$$\theta_I \equiv \beta - \alpha$$

where θ_I is positive when measured counterclockwise.

Then:

$$\beta = \alpha + \theta_I = \theta_I - \theta_H$$

and Equation (A1) becomes

$$\sin(\theta_I - \theta_H) + \sin \theta_H = \frac{n\lambda}{d}$$

The result for the $n = 0, \pm 1, \pm 2$ orders is shown in Figure A1c.

INITIAL DISTRIBUTION LIST

		No. Copies
1.	Defense Documentation Center Cameron Station Alexandria, Virginia 22314	20
2.	Library Naval Postgraduate School, Monterey, California	2
3.	Commander, Naval Air Systems Command Navy Department Washington, D. C. 20360	1
4.	Professor A. E. Fuhs Department of Aeronautics Naval Postgraduate School, Monterey, California	10
5.	Chairman, Department of Aeronautics Naval Postgraduate School, Monterey, California	1
6.	Ensign J. G. Sullivan, USN 16121 Northfield Street Pacific Palisades, California 90272	3
7.	Dr. L. O. Heflinger TRW Systems 1 Spacepark Avenue Redondo Beach, California 90278	1
8.	Dr. E. S. Lamar Chief Scientist Naval Air Systems Command Navy Department Washington, D. C. 20360	1
9.	Professor D. J. Collins Department of Aeronautics Naval Postgraduate School, Monterey, California	1
10.	Lt. J. H. Holds, USN 21 W. Goguac Street Battle Creek, Michigan 49015	1

11. Mr. K. G. Orman 1
Command Control and Guidance Administrator (Code 360)
Research and Technology
Naval Air Systems Command
Washington, D. C. 20360

12. Mr. I. H. Gatzke 1
Surveillance Administrator (Code 370)
Naval Air Systems Command
Navy Department
Washington, D. C. 20360

UNCLASSIFIED

Security Classification

DOCUMENT CONTROL DATA - R&D

(Security classification of title, body of abstract and indexing annotation must be entered when the overall report is classified)

1. ORIGINATING ACTIVITY *(Corporate author)*

Naval Postgraduate School
Monterey, California 93940

2a. REPORT SECURITY CLASSIFICATION

Unclassified

2b. GROUP

3. REPORT TITLE

AN INVESTIGATION OF THREE DIMENSIONALITY IN HOLOGRAPHIC INTERFEROMETRY

4. DESCRIPTIVE NOTES *(Type of report and inclusive dates)*

Thesis

5. AUTHOR(S) *(Last name, first name, initial)*

SULLIVAN, John G., Ensign, U. S. Navy

6. REPORT DATE	7a. TOTAL NO. OF PAGES	7b. NO. OF REFS
March 1968	78	21

8a. CONTRACT OR GRANT NO.	9a. ORIGINATOR'S REPORT NUMBER(S)
b. PROJECT NO.	
c.	9b. OTHER REPORT NO(S) *(Any other numbers that may be assigned this report)*
d.	

10. AVAILABILITY/LIMITATION NOTICES

Unlimited Distribution

This document is subject to special export controls and each transmittal to foreign nationals may be made only with prior approval of the Naval Postgraduate School.

11. SUPPLEMENTARY NOTES	12. SPONSORING MILITARY ACTIVITY

13. ABSTRACT

A discussion of the technique of holography and the laser light sources used therein is presented in this thesis as well as a mathematical description of intensity variation on a hologram due to diffraction and interference effects. Experimental verification is made that a dark-field, two beam hologram acts as a diffraction grating. Finally, the results of an experimental determination of intensity transmission functions for a light-field (diffuse glass) hologram are presented.

DD FORM 1 JAN 64 1473

UNCLASSIFIED

Security Classification

14 KEY WORDS	LINK A		LINK B		LINK C	
	ROLE	WT	ROLE	WT	ROLE	WT
HOLOGRAPHY OPTICS						
WAVEFRONT RECONSTRUCTION						
ELECTRO-OPTICS						
INTERFEROMETRY						
GAS DYNAMICS						